JOURNAL OF GEOPHYSICAL RESEARCH, VOL. 91, NO. B3, PAGES 3701-3723, MARCH 10, 1986

HEAT FLOW OBSERVATIONS ON THE BERMUDA RISE AND THERMAL MODELS OF MIDPLATE SWELLS

R. S. Detrick,[1] R. P. Von Herzen,[2] B. Parsons,[3] D. Sandwell,[4] and M. Dougherty[5]

Abstract. The Bermuda Rise is a broad topographic swell which is apparent in both residual depth and geoid anomaly maps of the western North Atlantic. The magnitudes of the depth and geoid anomalies associated with the Bermuda Rise are similar to the anomalies associated with other swells surrounding recent volcanic islands (e.g., Hawaii), suggesting that despite the lack of recent volcanism on Bermuda, the rise has a similar origin to other midplate swells. Results are reported from 171 new heat flow measurements at seven carefully selected sites on the Bermuda Rise and the surrounding seafloor. Off the Bermuda Rise the basement depths are generally shallower and the heat flow higher than either the plate or boundary layer models predict, with the measured heat flow apparently reaching a uniform value of about 50 mW m^{-2} on 120 m.y. old crust. On the Bermuda Rise the heat flow is significantly higher (57.4 ± 2.6 mW m^{-2}) than off the swell (49.5 ± 1.7 mW m^{-2}). The magnitude of the anomalous heat flux (8-10 mW m^{-2}) is comparable to that previously found along the older portion of the Hawaiian Swell near Midway. The existence of higher heat flow on both the Hawaiian Swell and Bermuda Rise indicates that these features fundamentally have a thermal origin. The differences in the shape, uplift, and subsidence histories of the Hawaiian Swell and Bermuda Rise can be quantitatively explained by the different absolute velocities of the Pacific and North American plates moving across a distributed heat source in the underlying mantle. Two-dimensional numerical convection models indicate that the observed depth, geoid, and heat flow anomalies are consistent with simple convection models in which the lower part of the thermally defined plate acts as the upper thermal boundary layer of the convection.

Introduction

The cooling and subsidence of the oceanic lithosphere as it ages can explain the principal features of the regional variation in seafloor depths [Parsons and Sclater, 1977]. However, there are many areas where the seafloor does not fit the expected depth-age relation [Menard, 1973; Anderson et al., 1973; Cochran and Talwani, 1978]. Most notable are the broad, topographic swells surrounding volcanic islands and island chains such as Hawaii, the Cook-Australs, Bermuda, and Cape Verde. These swells rise as much as 1000-1500 m above the surrounding seafloor and extend, in some cases, for several thousand kilometers along island chains [Morgan, 1972; Watts, 1976; Detrick and Crough, 1978; Crough and Jarrard, 1981]. They are typically associated with long-wavelength (~2000 km), positive gravity anomalies of a few tens of milliGals and geoid anomalies of up to about 10 m [Crough, 1978].

The origin of these features remains controversial; however, the observation that midplate swells, and the atolls and guyots formed on them, subside according to a predictable thermal cooling curve [Detrick and Crough, 1978; Menard and McNutt, 1982] indicates that these swells fundamentally have a thermal origin. If the formation and subsequent disappearance of swells are controlled by thermal processes, then portions of the swell should have an above normal heat flux [Crough, 1978]. The size and location of this heat flow anomaly will depend on how temperature changes within the thermal plate occur and provide important constraints on possible reheating mechanisms.

The Hawaiian Swell is the only such feature for which reliable heat flow data have been published [Detrick et al., 1981; Von Herzen at al., 1982]. Measurements were made at eight sites along the swell and the heat flow was observed to increase systematically from near-normal values at Hawaii to values near Midway 7-12 mW m^{-2} higher than the expected heat flow for crust of this age. Although this anomaly is small, it represents approximately 20-25% of the normal background heat flux and is statistically resolvable with the data collected. These observations are consistent with a rapid temperature increase in the lower half of the thermally defined plate, leaving the near-surface temperatures unaffected initially. Then as the heat input diffuses upward it gradually raises shallow temperatures, creating an increased surface heat flux as the swell cools and subsides. Because of the rapid motion of the Pacific plate, the thermal anomaly is swept downstream of the Hawaiian hot spot by the moving lithosphere and is not observed as a surface heat flow anomaly until some 20 m.y. later [Detrick et al., 1981; Von Herzen et al., 1982].

Although the spatial and temporal separation of the heat source and the surface heat flow anomaly at Hawaii provides an important constraint on the depth of the initial temperature changes, it also complicates the interpretation of these data. It is difficult, for example, to be certain that the full magnitude of the heat flux anomaly has been determined, and only additional data along and across the Hawaiian Swell could confirm this. Another uncertainty in this study is that reliable

[1]Graduate School of Oceanography, University of Rhode Island, Kingston.
[2]Department of Geology and Geophysics, Woods Hole Oceanographic Institution, Woods Hole, Massachusetts.
[3]Department of Earth, Planetary and Atmospheric Sciences, Massachusetts Institute of Technology, Cambridge.
[4]National Geodetic Survey, National Ocean Service, NOAA, Rockville, Maryland.
[5]Massachusetts Institute of Technology/Woods Hole Oceanographic Institution, Woods Hole.

Paper number 5B5651.
0148-0227/86/005B-5651$05.00

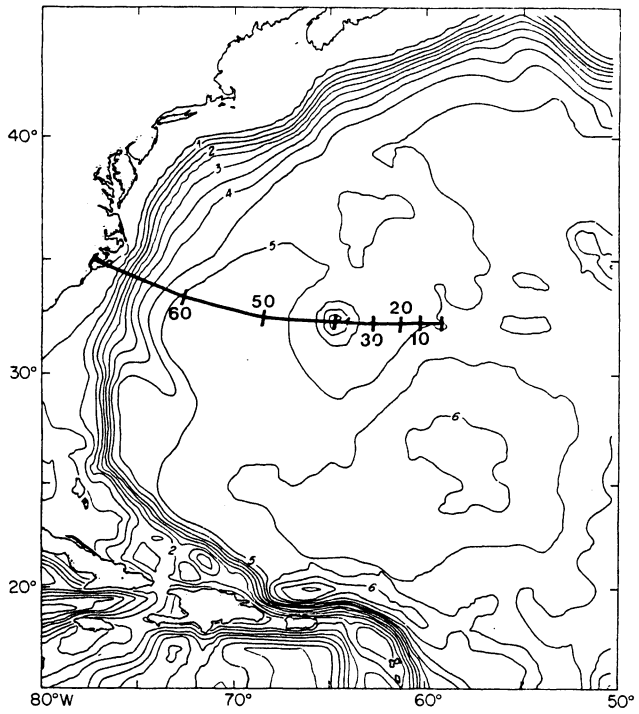

Fig. 1. Bathymetry of the western North Atlantic derived from the SYNBAPS data base by smoothing and interpolating depth values onto a uniform 50 km grid using a function defined by $N_i = [\Sigma w_{ij} n_j]/\Sigma w_{ij}$ and $w_{ij} = \exp(-r_{ij}^2/\sigma^2)$, where r_{ij} is the distance from a grid point i to data points j [McKenzie et al., 1980]. The Gaussian weighting function w_{ij} was used with a 50-km half width. Contour interval 0.5 km. The Bermuda Rise, located at about 32°N, 65°W, is approximately defined by the 5-km depth contour. Solid line shows Morgan's [1983] predicted track for the Bermuda hotspot with ages indicated in m.y. B.P.

heat flow measurements were not obtained off the swell for comparison. Thus it is not certain that the heat flow on the swell is higher than crust of the same age located off the swell.

In this paper we present the results from a similar heat flow investigation of the Bermuda Rise in the western North Atlantic. Unlike Hawaii, the motion of the North American plate over the Bermuda hotspot is small [Morgan, 1983], and sufficient time should have elapsed since the formation of the swell in the middle Eocene [Tucholke and Mountain, 1979] for the heat flow anomaly to be well developed. Thus at Bermuda it may be possible to obtain a more reliable measure of the peak heat flow associated with the swell. The main uncertainty at Bermuda is the absence of recent volcanic activity [Reynolds and Aumento, 1974] which may indicate a waning of the strength of the hotspot over the past 20-30 m.y.

In the following sections we review the known geological history of the Bermuda Rise, describe the new heat flow measurements that we obtained on the swell, and present thermal and numerical convection models that explain these results and the major differences in the uplift and subsidence history of the Bermuda Rise and Hawaiian Swell.

Bermuda Rise

The Bermuda Rise is a NE-SW trending topographic high about 900 km long and 600 km wide that is approximately delineated by the 5000-m depth contour (Figure 1). It is bordered by the Hatteras Abyssal Plain to the west, the Nares Abyssal Plain to the south, and the Sohm Abyssal Plain to the north and east. The Bermuda Rise is clearly apparent in both residual depth [Sclater and Wixom, 1985] and geoid anomaly maps (Figure 2) of the western North Atlantic as a broad, slightly oblate feature with a wavelength of about 2000-3000 km. The peak residual depth and geoid anomalies approximately coincide and have maximum values of 800-1000 m and 6-8 m, respectively. The geoid and depth anomalies over the Bermuda Rise are similar in magnitude to the anomalies associated with other swells surrounding recent volcanic islands (e.g., Hawaii), suggesting that despite the lack of recent volcanism on Bermuda, the mode of origin of the Bermuda Rise is the same as for these other swells. Curiously, however, the NE-SW orientation of the Bermuda Rise is nearly orthogonal to Morgan's [1983] predicted track of the Bermuda hotspot (Figure 1).

Bermuda is the largest of three volcanic seamounts near the crest of the rise that trend 035° [Johnson and Vogt, 1971]. The islands have a maximum elevation of only 30 m and occupy the southeastern 7% of the 116 km^2 Bermuda platform. Only limestones are exposed on the islands, but seismic reflection profiles [Gees and Medioli, 1970] suggest that the top of the basaltic plat-

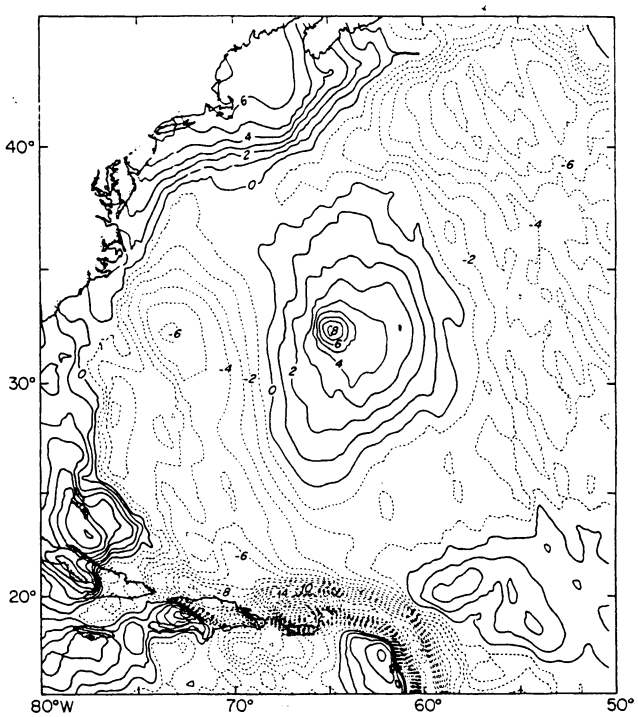

Fig. 2. Geoid anomalies in the western North Atlantic derived from Seasat altimeter data after removing a GEM 9 reference field up to degree and order 10 and smoothing and interpolating the resulting geoid anomalies onto a uniform 50-km grid by using the same method as for the bathymetry data in Figure 1. Contour interval 1 m.

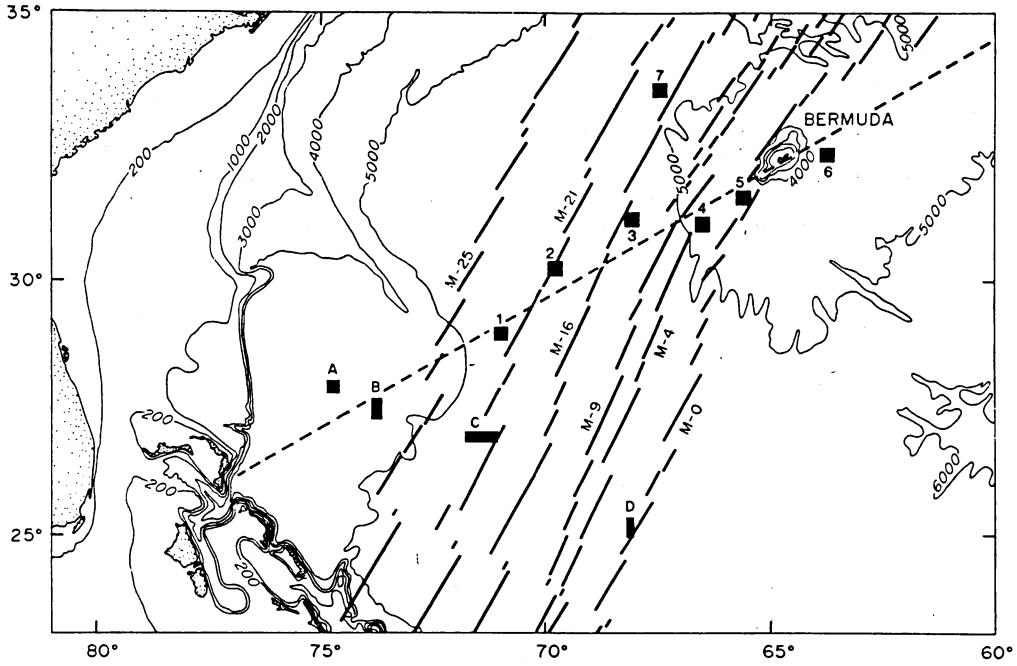

Fig. 3. Map of the Bermuda area showing the location of our sites 1-7. Sites A-C are from Davis et al. [1984], site D is from Galson and Von Herzen [1981]. Dashed line shows location of profile in Figure 11. Magnetic anomaly identifications are from Klitgord and Schouten [1985] and M. T. Sundvik (manuscript in preparation, 1985).

form is an average of about 76 m below sea level with the shallowest depths located near the Bermuda Biological Station where a drill hole in 1972 reached volcanics 26 m below sea level [Aumento and Ade-Hall, 1973]. Over 700 m of tholeiitic lavas and intrusive lamprophyric sheets were drilled at this site. The intrusives were dated at about 33 Ma; the lavas may be substantially older, but because they have undergone extensive hydrothermal alteration, age dating is difficult [Reynolds and Aumento, 1974].

The early volcanic history of Bermuda and the timing of the initial uplift of the Bermuda Rise have been determined from studies of sediments deposited on the rise [Tucholke and Mountain, 1979]. Middle and lower Eocene sections at Deep Sea Drilling Project (DSDP) drill sites on the western and central Bermuda Rise contain numerous graded beds (horizon A^T) which are interpreted as turbidites derived from the eastern U. S. continental margin. Above horizon A^T the upper Eocene sediments on the rise are pelagic oozes and lack graded bedding. This abrupt transition from turbidite to nonturbidite deposition on the western Bermuda Rise is interpreted by Tulcholke and Mountain [1979] as evidence for the initial uplift of the swell beginning in the middle Eocene (45-50 Ma). Volcaniclastic turbidites at DSDP Site 386, 140 km southeast of Bermuda, show that the Bermuda volcanoes had reached sea level and were being actively eroded by the late-middle Eocene to early Oligocene (35-43 Ma). These turbidites form a strong reflector, A^V, closely overlying horizon A^T, within about 250 km of Bermuda. At DSDP site 386 the top of the turbidites date to the late Oligocene (25 Ma), indicating the end of significant subaerial erosion and the subsidence of the volcanic platform below sea level. The limestone reef cap on Bermuda is poorly dated but is probably entirely of Miocene age.

The above description suggests the following geological history for the Bermuda Rise: A heating event leading to the uplift of the swell occurred in the middle to late-middle Eocene followed by the volcanism that formed Bermuda. This volcanism continued until the end of the early Oligocene. The volcanic platform sunk below sea level in the late Oligocene, ending significant subaerial erosion. A small amount of subsidence has occurred since the early Miocene allowing the Bermuda platform to be covered by a thin coral reef cap.

Heat Flow Measurements

Although the western North Atlantic has been well-surveyed, the number of published heat flow measurements in the region is not correspondingly large. Between 20°N and 40°N west of the Mid-Atlantic Ridge, an area of some 7×10^6 km^2, there are less than 150 heat flow measurements and many of these are concentrated near the Mid-Atlantic Ridge (crust <30 Ma). Over the Bermuda Rise (defined by the 5-km depth contour in Figure 1) there are only 16 measurements.

From the existing values the mean heat flow on the Bermuda Rise is 51.5 ± 9.6 mW m^{-2} (1.23 ± 0.23 μcal cm^{-2} s^{-1}). The heat flow measured in a drill hole on Bermuda is somewhat higher, about 53-57 mW m^{-2} [Hyndman et al., 1974]. By comparison, the mean of 38 stations around the Bermuda Rise, within about 500 km of the bounding 5 km depth contour but deeper than 5 km, is 48.2 ± 11.7 mW m^{-2} (1.15 ± 0.28 μcal cm^{-2} s^{-1}). Thus within the uncertainty in the existing data, the heat flow

on the Bermuda Rise is not significantly different than that off the Bermuda Rise.

There are reasons, however, to doubt the reliability of these measurements. Sediment thermal conductivities are not well determined at many stations, either having been assumed or estimated from nearby sites. Possible environmental effects including local refraction of conducted heat by seafloor or sediment-basement topography [e.g., Galson and Von Herzen, 1981], slumping of sediments initially deposited on topographic slopes [Von Herzen and Uyeda, 1963; Birch et al., 1968], and, most importantly, the loss of heat through permeable basement rock outcrops by hydrothermal circulation [Lister, 1972; Anderson et al., 1977] generally have not been evaluated for most stations. The last effect is especially important with the rough basement topography in much of the western North Atlantic and evidence that the thermal regime can be disturbed up to distances of 20-30 km from the basement outcrops [Embley et al., 1983]. Surveys to determine the presence of nearby basement outcrops are nonexistent for almost all published data from the Bermuda Rise.

The strategy employed in the experiment reported here is to concentrate the heat flow measurements in a few well-surveyed sites to minimize the possibility of environmental disturbances. This technique was successful in revealing the relatively small heat flow anomaly over the Hawaiian Swell, where none had been obvious before, and the anomaly associated with Bermuda should be of comparable magnitude.

Site Locations and Surveys

Heat flow measurements were made in seven well-surveyed sites (Figure 3). Six of the seven sites comprise a profile extending approximately southwest of Bermuda, from the Hatteras Abyssal Plain (site 1) to the shallowest part of the Bermuda Rise (site 6). Site 7 was placed to the northwest of Bermuda to determine if a similar thermal gradient exists across the swell in that direction. The location and orientation of this profile were based on several criteria: (1) the generally high density of survey track data west of Bermuda, allowing good control on seafloor age (magnetic anomalies) and fracture zone locations; (2) relatively uniform and thick ($\geq$ 1 km) sediment cover west of Bermuda; (3) a steep gradient in the geoid anomaly associated with the Bermuda Rise in this direction (Figure 2); and (4) the existence of recently surveyed heat flow sites on older crust off the swell southwest of Bermuda [Galson and Von Herzen, 1981; Davis et al., 1984].

The sites were chosen along the profile at intervals of 100-200 km. As in the Hawaiian Swell investigation, a bathymetric and seismic reflection survey was carried out at each site over an area nominally 20 km on a side to establish the basement topography and the continuity and thickness of the sediment cover (see Figures A1-A7 in microfiche appendix[1]). Following the seismic survey at each site, two piston cores were obtained to determine the thermal conductivity of the surficial sediments, and thermal gradients were measured over the survey area with a "pogo" probe.

Navigation for the entire experiment was determined from LORAN-C and transit satellite signals received aboard the vessel. Reception of LORAN-C was nearly continuous throughout the field work, somewhat noisier (more variable) at night, but sufficient to establish relative positions at each site to 0.2 km or better. However, systematic discrepancies were found between LORAN-C and satellite positioning of up to 3 or 4 km. This bias, which was uniform within each site but different between sites, is probably caused by variable time delays in transmission of signals between LORAN-C stations and the vessel, perhaps associated with land topography. All LORAN-C positions (Table A1, appendix) were corrected for the mean offset between all good satellite and LORAN-C positions at each site. Also, the station positions were taken as that of the vessel at the time of measurement. Although we attempted to minimize lateral offset between the bottom instrumentation and the surface vessel by maneuvering for vertical wire angles at the time of measurement, we have some evidence (site 5, see below) of systematic offsets up to 1 km or so, depending on the magnitude and direction of the vessel motion between pogo measurements. We have not made any corrections to station positions to account for these possible offsets.

The bottom topography is relatively subdued at all sites, varying from about 160 m at site 5 to less than 7 m at site 1 in the Hatteras Abyssal Plain. However, the amplitude of basement topography beneath the sediments is usually much greater, up to 1 km or more, particularly at sites near Bermuda (4, 5, 6), and is weakly lineated parallel to the magnetic anomaly directions (NNE). Therefore the sediment thickness, rather than the bottom depth, was contoured at each site (Figures A1-A7, appendix). As an example, the survey and station locations for site 5 are shown in Figure 4. No basement outcrops were detected at any of the sites, although a hill and near-outcrop were crossed about 20 km from the nearest heat flow measurements at site 7. The effect of this feature on nearby heat flow measurements appears minimal (see below).

Temperature Gradients Measurements

Gradients were determined from measurements with outrigged thermistor sensors attached to a "pogo" probe similar to that described by Von Herzen et al. [1982]. Two probe configurations were employed, depending on the penetrability of the surficial sediments: one with seven thermistor sensors mounted over 7 m length and the other with four thermistors spaced over a probe about 3.5 m in length. The instrumentation is otherwise quite similar to that described by Von Herzen et al. [1982]. Other significant differences included measurements of tilt to high precision at all stations and of in situ thermal conductivity on more than one third of all penetrations (see below). Tilt of the instrument was measured with a liquid sensor each recording cycle (~30 s) along two orthogonal axes.

The total number of successful gradient pene-

[1]Appendix is available with entire article on microfiche. Order from the American Geophysical Union, 2000 Florida Avenue, N.W., Washington, DC 20009. Document B86-002; $2.50. Payment must accompany order.

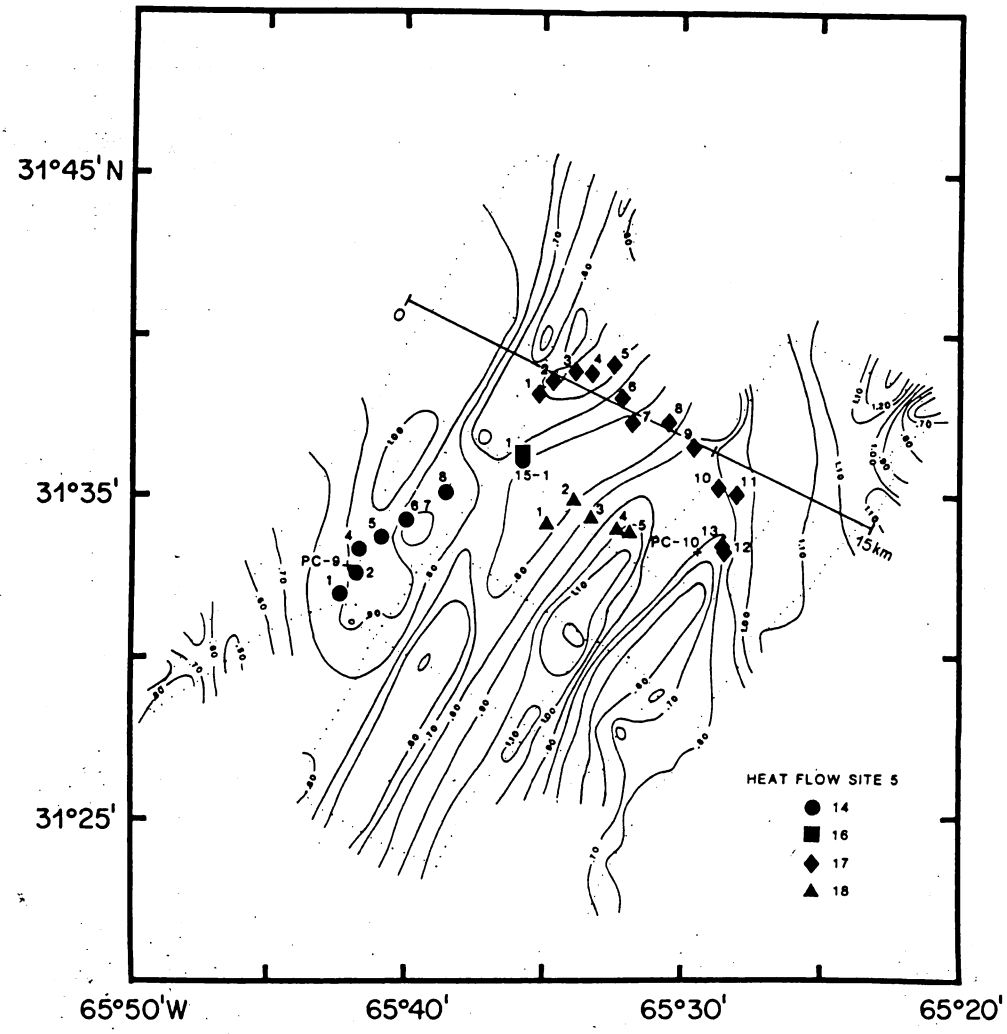

Fig. 4. Example of detailed survey data and stations at site 5. Contours are two-way reflection time in seconds from the seafloor to acoustic basement. Pogo probe temperature gradient stations are indicated by solid geometric symbols; piston cores by crosses. Heat flow and basement depths along the line shown in Figure 9.

trations was 171, ranging from 11 at site 1 to 35 at site 7. To reduce the statistical uncertainty and to average out any variations due to the environment (basement topography, etc.), it is desirable to obtain at least 20-30 measurements spaced as uniformly as possible over the survey site. In practice, pogo stations are usually aligned as profiles along a direction favorable for moving the vessel, although there is usually some latitude in maneuverability to allow crossed patterns (Figure 4). Initial instrumentation difficulties and indurated turbidite sediments prevented more measurements at site 1.

Examples of the measured gradients are given in Figures 5 and 6. Temperature uncertainties (95% confidence) associated with each data point are derived from the uncertainties in extrapolation of probe temperature to equilibrium after the initial penetration heating pulse, as well as sensor noise and stability determined from temperatures recorded while instrumentation was suspended in the nearly isothermal bottom water. In general, gradients determined from three or more subbottom equilibrium temperature measurements show little, if any, departure from linearity. Together with the bottom water temperature, these gradients were also used to determine the depth of penetration.

Combined with relatively constant thermal conductivity over depth (see below), these gradients likely reflect conditions of steady state heat flux. Gradient values (Table A1, appendix) are determined from the best linear fit through the temperature points of each measurement, weighted inversely proportional to the square of their uncertainties. The mean gradient for each site, given in Table 1, is a weighted average of the station gradients, each individual gradient measurement being weighted inversely proportional to its uncertainty. Other weighting schemes (e.g., equal weight) do not change the site means more than a few percent. The site heat flow means (Table 1) have been calculated from the individual station values.

Thermal Conductivity Measurements

Conductivity was determined from needle probe measurements [Von Herzen and Maxwell, 1959] on recovered sediment cores, as well as in situ with a scaled-up version of the needle probe method

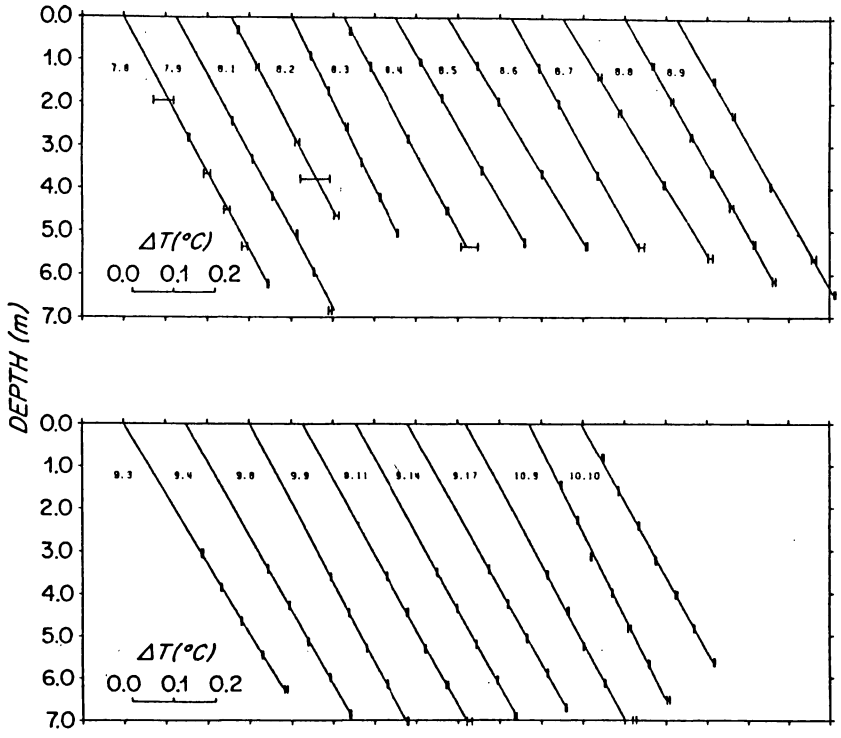

Fig. 5. Representative temperature gradients at several stations at sites 2 and 3. For display purposes, successive measurements are displaced 0.1°C in bottom water temperature. Error bars give 95% confidence limits in equilibrium temperatures. The linear gradients are indicative of purely conductive heat loss.

utilizing the same thermistor probes employed in gradient determinations [J. Jemsek and R. P. Von Herzen, manuscript in preparation, 1985]. Two piston cores recovered from each site were used for the shipboard laboratory measurements of conductivity (Table A2, appendix). Core recovery was excellent, averaging about 11 m of recovered sediments, and measurements were made approximately at 30-cm intervals (Table A3, appendix). The in situ values were obtained at all sites except site 1, where the turbidites and malfunctioning instrumentation prevented their acquisition.

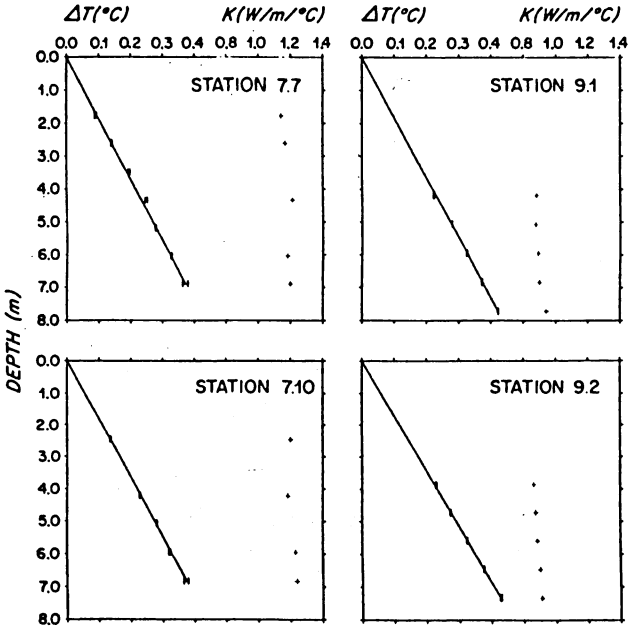

Fig. 6. Temperature gradients and in situ thermal conductivity measured at four pogo stations at sites 2 and 3.

Although there are significant differences in mean conductivity between sites, little systematic variation with depth is obvious at any site to the maximum depth of probe penetration (8 m) (Figures A8-A21). The systematic depth variation was obscured at site 1 because of larger variability over short distances associated with the turbidite sediments of the abyssal plain. Any large-scale depth variations inferred from the measurements on cores at that site may be aliased by inadequate sampling of small-scale variability. Nevertheless, the mean conductivity values of the two cores recovered at site 1, separated by about 15 km, are nearly equal, giving us confidence that we have adequately sampled the cores and have determined a mean conductivity representative of the site.

However, unlike the data on the Hawaiian Swell, the mean values of each core are not always within the confidence limits (95%) of the mean for the other core at each site. Statistically significant differences between mean core values were measured at Sites 2, 4, and 6, amounting to 6%, 8%, and 8% of the site means, respectively. We believe that these results indicate variations in conductivity of this magnitude over short distances (less than a few kilometers) for at least these sites, emphasizing the importance of in situ measurements.

The in situ conductivity values were obtained

TABLE 1. Bermuda Rise Heat Flow: Site Summary

Site	Location	Age, Ma	Depth, km	N_G	Gradient, °C/km	N_C	Thermal Conductivity: Cores, W m^{-1} K^{-1}	N_I	Thermal Conductivity: In Situ, W m^{-1} K^{-1}	Heat mW m^{-2}
1	29°00'N 71°00'W	152	6.0±0.1	11	46.5±2.2	68	1.087±0.041	-	-	50.7±2.5
2	30°15'N 69°45'W	150	5.8±0.1	27	55.2±1.1	48	0.932±0.012	4	0.905±0.055	51.8±1.3
3	31°10'N 68°03'W	140	5.7±0.1	27	56.1±1.1	59	0.917±0.013	18	0.914±0.011	51.0±0.8
4	31°03'N 66°30'W	125	5.6±0.2	22	65.2±2.9	49	0.927±0.020	10	0.950±0.040	58.9±1.9
5	31°35'N 65°35'W	119	5.2±0.1	27	49.4±1.7	53	1.032±0.018	19	1.112±0.029	54.4±2.3
6	32°23'N 63°45'W	112	4.9±0.1	22	55.3±2.3	51	0.996±0.021	5	1.081±0.037	58.8±2.6
7	33°37'N 67°25'W	143	5.5±0.1	35	54.9±1.2	59	0.934±0.008	8	0.922±0.039	50.1±1.1
A	27°56'N 74°42'W	162	5.9±0.1							49.0±1.7
B	27°25'N 73°46'W	159	5.6±0.1							47.0±1.5
C	26°54'N 71°24'W	151	6.0±0.1							49.0±1.0
D	25°00'W 68°00'W	119	5.8±0.1							47.3±2.1

Location is approximate center of surveyed region; A-C from Davis et al. [1984]; D from Galson and Von Herzen [1981]. Ages based on geomagnetic polarity time scale of Kent and Gradstein [1985]. Depths are average basement depth at each site corrected for sediment loading using the correction factor given by Crough [1973]. N_G is number of gradients measured at each site. N_C is number of needle probe measurements on cores. N_I is number of stations with in situ conductivity measurement. All uncertainty ranges given at the 95% confidence level.

at the same locations where gradients were measured, after dissipation of the transient heating of the probes caused by the bottom penetration. A microprocessor was used to control the initiation and duration of a steady electrical current applied to a resistance wire installed within the thermistor probe. The heating element was sometimes mounted in a separate tube parallel to the main thermistor probe, a configuration designated the "double probe." The increase of temperature at each probe is measured over a period of 10 minutes of heating while in the bottom. The data are analyzed by a computer program which accounts for the initial heating transient associated with bottom penetration, as well as the finite size and thermal inertia of the probe array [J. Jemsek and R. P. Von Herzen, manuscript in preparation, 1985]. The uncertainties in the absolute value of conductivity determined by the single probe are estimated at 3-5% and for the double probe at 5-6%

A total of 346 in situ measurements of thermal conductivity were obtained on 64 penetrations at sites 2-7 (Table A1, appendix). The number of penetrations with in situ measurements ranged from 4 at Site 2 to 19 at site 5. The mean in situ conductivities at each site are given in Table 1, where they are compared with the mean core values corrected for ambient pressure and temperature at the sea floor [Ratcliffe, 1960]. All means calculated are unweighted by any uncertainties in the measured values since the square of the uncertainties in fitting the heating curves is generally of the order of 1% or less; any poorer fitting measurements were usually discarded.

The site mean in situ conductivities are within the uncertainty range of at least one core mean value at four sites (2, 3, 4, and 7) where they were both measured. However, at the two other sites (5 and 6) the in situ mean values are higher than the needle probe values on cores by 8% and 9%, respectively. We note that the mean conductivity is highest at these two sites among those where both measurement techniques were successful

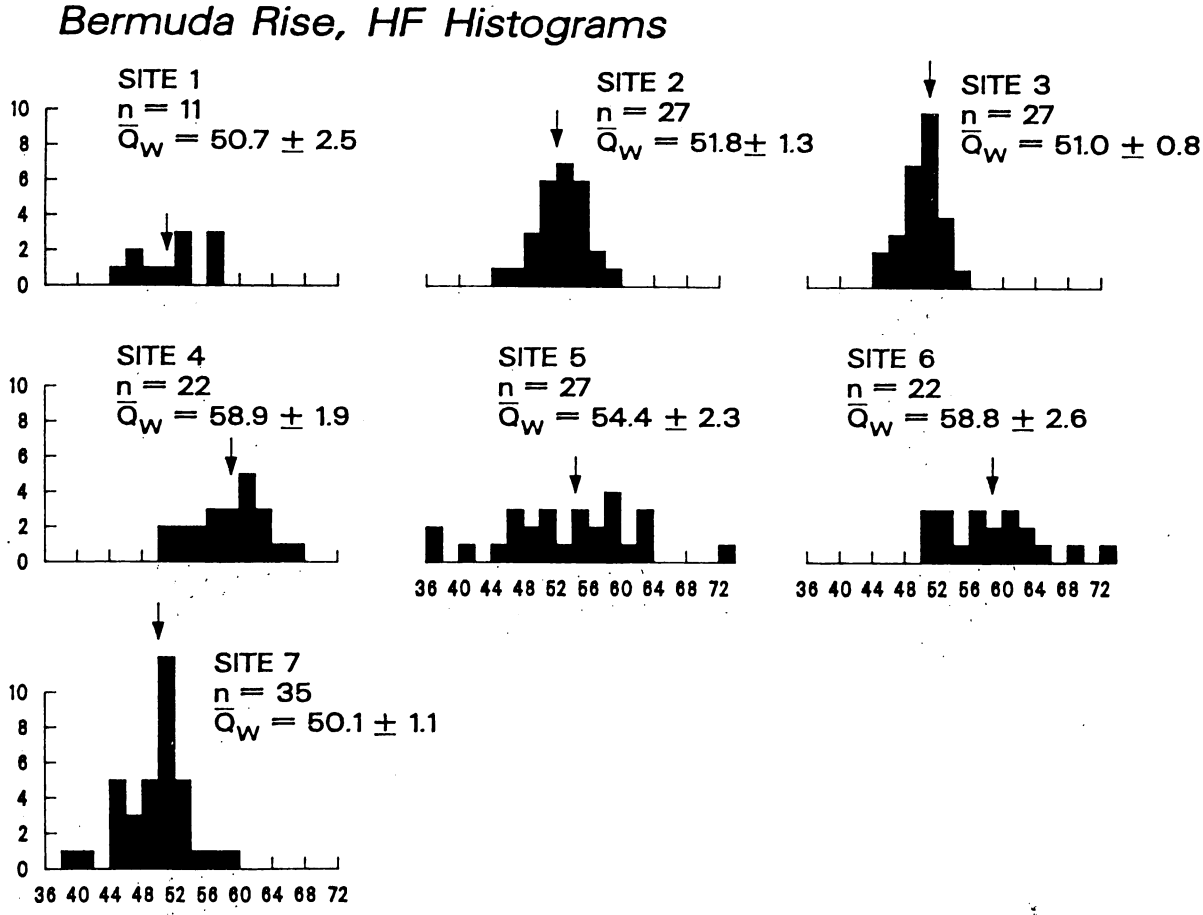

Fig. 7. Histograms of heat flow data obtained at each site (Table A1, appendix). Heat flow values in mW m^{-2}. N indicates the number of stations at each site, and $\bar{Q}_w$ is the weighted mean heat flow at each site.

and that the double probe method of in-situ measurements was primarily used at both sites. Although the evidence from these and other in situ measurements [J. Jemsek and R. P. Von Herzen, manuscript in preparation, 1985] indicates that the in situ double probe method gives unbiased values with slightly increased uncertainty compared to the single probe, we consider below the implications of some possible bias in the in situ method for higher conductivities.

Heat Flow Calculations

The station heat flow values are calculated as the product of the gradient G and the mean thermal conductivity K, either locally determined in situ or from the site mean K if no in situ measurements were obtained at the station. The site mean K was calculated from an unweighted average of all available conductivity measurements (both core and in situ) at the site. The uncertainty range of the heat flow value is calculated as [Von Herzen, et al. 1982]

$$\Delta Q = K\Delta G + G\Delta K \quad (1)$$

where ΔG and ΔK are the uncertainty ranges, calculated at the statistical 95% confidence level, in the gradient and thermal conductivity, respectively (Table A1, appendix).

As in the case of the Hawaiian Swell data, the acquisition of numerous measurements within well-surveyed regions of limited extent give remarkably small uncertainty ranges to the site means (Table 1). The site mean heat flow values in Table 1 are a weighted average of the station heat flow values (Table A1, appendix). Weights inversely proportional to the uncertainties in station heat flow values were used, but other weighting schemes (e.g., equal weight) do not change the site means values by more than 1 or 2 mW m^{-2}, with comparable uncertainties. Even at site 1 with fewer gradient measurements (11), the uniformity of values gave uncertainties comparably small to the other sites with more numerous, but sometimes more variable, station data. The histograms of heat flow values acquired at each site are shown in Figure 7. At some sites (e.g., site 5) the data are obviously more variable than at others (e.g., site 3).

The most in situ conductivity data were obtained at sites 3 and 5, and accordingly, the station conductivity values have been plotted against station gradients for these two sites in Figure 8. If heat flow were constant for a site, then these points should plot along curves of constant heat flux. Indeed, this seems to be the case at site 3, where the relatively small scatter probably reflects the small experimental uncertainty of gradient measurements at this site (Table 1). Site 5 shows not only a significantly larger range of variation in both gradient and conductivity values but also a scatter in station

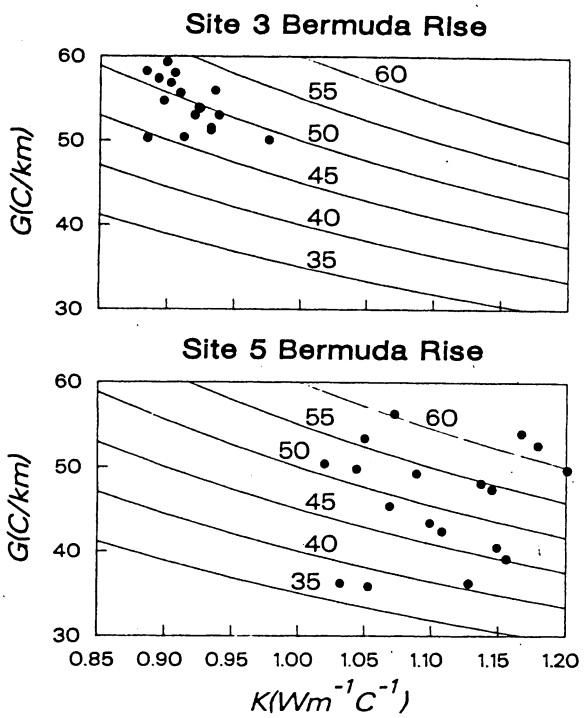

Fig. 8. Contours of heat flow in mW m^{-2} as a function of temperature gradient G and in situ thermal conductivity K with the measured station values at sites 3 and 5 indicated by solid circles. If the heat flux were constant for a site, then these points should plot along curves of constant heat flow. This seems to be the case at site 3, but at site 5 the variability is significantly greater than can be explained by experimental uncertainty.

heat flow values a factor of 5-10 larger than for site 3. The variability at Site 5 is significantly greater than can be explained by experimental uncertainty.

The source of much of the variability in heat flow at site 5 is seen in Figure 9. This profile shows the systematic variation in heat flow across part of this site, with an apparent wavelength of 5-6 km. Furthermore, the pattern of heat flow variability correlates well with the two-dimensional basement topography, although slightly displaced from it (1-1.5 km). We note that the measured heat flow pattern is shifted in the direction the vessel is moving for the "pogo" penetration profile. It seems probable that the bottom instrumentation "follows" the vessel by the amount of shift between the profile, which seems reasonable for the water depth (~5 km), and that the heat flow extrema actually correlate in position with the basement topography.

We have used a finite element thermal model [Lee and Henyey, 1974] to investigate the amplitude of the expected heat flow variations due to basement topography at site 5. The results (Figure 9) indicate that the expected conductive heat flow variations for site 5 are significantly smaller than actually measured. It seems improbable that any reasonable changes in the model parameters can account for this discrepancy. The observed heat flow pattern also cannot be explained by maintaining basement at a constant temperature. Basement temperatures at this site extrapolated from the observed heat flow measurements and estimated sediment thicknesses range from about 24° to 38°C with little correlation with basement topography. This basement temperature variation of almost a factor of 2 is similar to the 100°-200°C range in basement temperatures found by Davis and Lister [1977] on the Juan de Fuca Ridge, although lower in amplitude. Even though the statistical uncertainty at site 5 is small, it is not clear that our spatial coverage is adequate to define the mean heat flux, and we are not certain to what extent the mean value may be affected by vertical advection through basement outcrops outside (but nearby) the surveyed region.

An attempt was made to investigate the influence of basement outcrops on the heat flux at site 7 (Figure A7, appendix). A small basement outcrop, or near outcrop, was crossed along the track to the site, about 20 km to the southeast of the site. The mean of the 7 values (stations 24.1-24.7) obtained near and on this feature, 50.4 mW m^{-2}, is not significantly different from the site mean. The values also have about the same variability as the other values obtained at this site. If hydrothermal circulation were active in the basement, we would expect either a higher or lower mean value near the outcrop, depending on the direction of water flow into or out of the permeable basement rock, and probably increased variability in the heat flux values. Therefore we conclude that hydrothermal circulation does not appear active at this site. We cannot discount the possibility that convective heat loss is important at some of the other sites (e.g., site 5), but given the linear temperature gradients and relatively uniform sediment cover at most sites, we do not believe that our measurements are seriously biased by these effects.

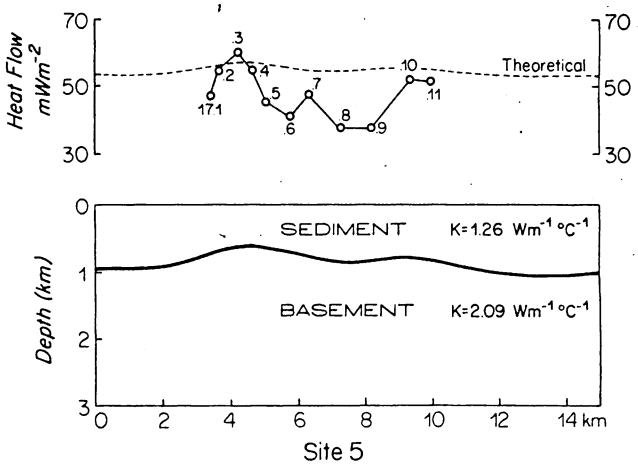

Fig. 9. Profile of theoretical and observed heat flow at site 5. Theoretical curve (dashed line) computed using the model of Lee and Henyey [1974] from the two-layer conductivity structure shown with uniform heat flow at 10 km depth equal to site mean heat flow (54.4 mW m^{-2}). Observed values are projected into the profile (Figure 4) and shifted 1 km to the left to allow for displacement between the heat flow probe and the ship.

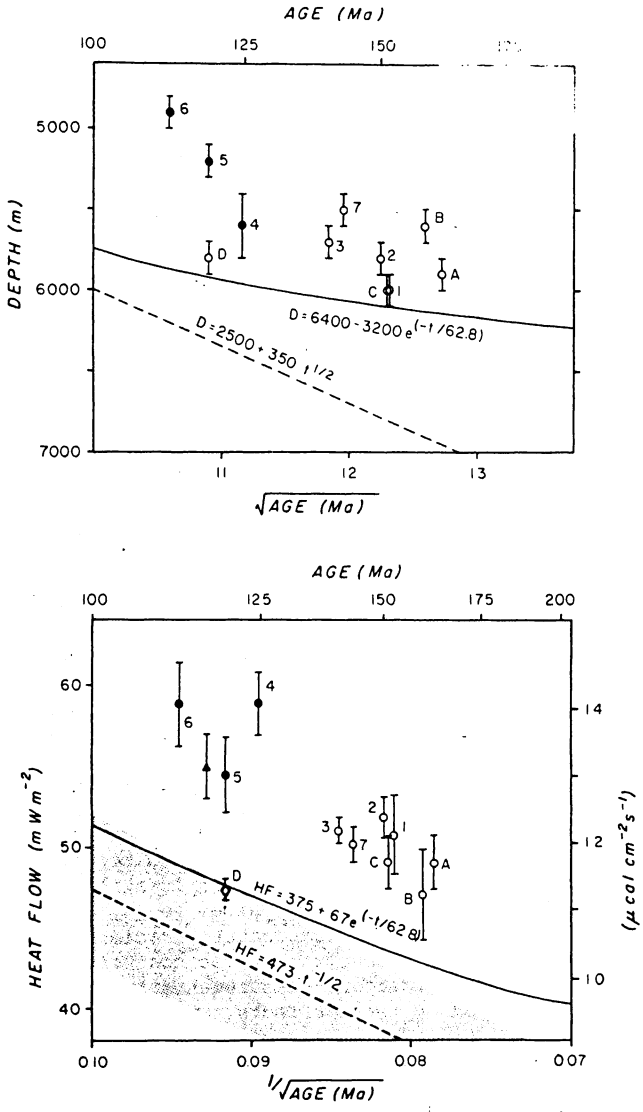

Fig. 10. Average basement depths corrected for sediment loading (top) and heat flow with 95% confidence limits (bottom) at sites on (solid symbols) and off (open symbols) the Bermuda Rise plotted versus age. Unlabeled solid triangle is heat flow value measured in a borehole on Bermuda by Hyndman et al. [1974]. Empirical curves for plate and boundary layer cooling models [Parsons and Sclater, 1977] are shown for comparison.

Another uncertainty in the heat flow measurements at sites 5 and 6 is the different mean values of laboratory and in situ thermal conductivity. Although we believe that these differences reflect local variability in conductivity at these sites and that the in situ values are unbiased, a conservative approach is to assume that only the lower, mean conductivity values of the needle probe measurements are valid. In this case, the heat flow means at sites 5 and 6 defined by the product of the mean gradient and mean core conductivity (Table 1) are 51.0 ± 2.6 and 55.1 ± 3.5 mW m^{-2}, respectively, the calculated mean for site 5 is then very close to the lower values on the Hatteras Abyssal Plain (site 1) and those of the lower Bermuda Rise flank (sites 2, 3, and 7), whereas the mean at site 6 remains significantly higher. Although we consider this interpretation to be less likely in view of the in situ conductivity data, it remains a possibility and would have been our conclusion without the in situ measurements.

Discussion of Heat Flow Results

The unloaded basement depths and mean heat flow at each site are plotted against age in Figure 10, where they are compared with the empirical depth and heat flow versus age relations given by Parsons and Sclater [1977] for both the boundary layer and plate cooling models. Also shown are data from four other detailed, multipenetration heat flow determinations (sites A-D) located south and west of Bermuda [Galson and Von Herzen, 1981; Davis et al., 1984] (see Figure 3 for location) which provide additional control on the heat flow off the Bermuda Rise. The age at each site was determined from Klitgord and Schouten's [1985] and M. T. Sundvik's (manuscript in preparation, 1985) magnetic anomaly identifications in this area using the geomagnetic polarity time scale of Kent and Gradstein [1985]. Sediment loading corrections were estimated from seismic reflection data at each site using a factor of 600 m s^{-1} of two-way reflection time to basement [Crough, 1983a] and are probably accurate to ±100 m.

A surprising result, previously noted by Davis et al. [1984] is that even off the Bermuda Rise the basement depths are generally shallower and the heat flow higher than either the plate or boundary layer models predict. Site D of Galson and Von Herzen [1981] is the only site at which both the depth and heat flow lie relatively close to one of the empirical relations. The depths at the seven other off-swell sites average about 300-400 m shallower than predicted by the plate model and over 1000 m shallower than predicted by the boundary layer model, while the heat flow at the older sites is about 15% higher than expected. Moreover, the heat flow appears to have approached an equilibrium value of about 48-50 mW m^{-2} by 120 Ma, a much earlier departure from the $t^{-1/2}$ relationship than that predicted by the plate model.

Some bias has been introduced into this comparison by the different geomagnetic time scales and sediment-loading corrections employed in this study compared to that used by Parsons and Sclater [1977] to derive the empirical depth and heat flow versus age relations. For example, the Kent and Gradstein [1985] time scale assigns an age of 150 Ma to anomaly M21 compared to 145 Ma in the Larson and Hilde [1975] time scale used by Parsons and Sclater [1975]. However, this introduces an error of no more than 1% in the predicted depth and heat flow which is clearly insignificant. More important are differences in the sediment-loading corrections. Parsons and Sclater [1977] assumed a constant sediment density of 1.7 g/cm^3, which overestimates the corrected basement depths for sediment thicknesses greater than a few hundred meters [LeDouaran and Parsons, 1982]. Using the correction factor derived by Crough [1983a], the empirical depth-age curves should be shifted shallower by about 90-150 m for sediment thicknesses of 0.8-1.4 s two-way travel time (typical of the older sites plotted in Figure 10). This accounts for part, but not all, of the discrepancy apparent between the observed and predicted base-

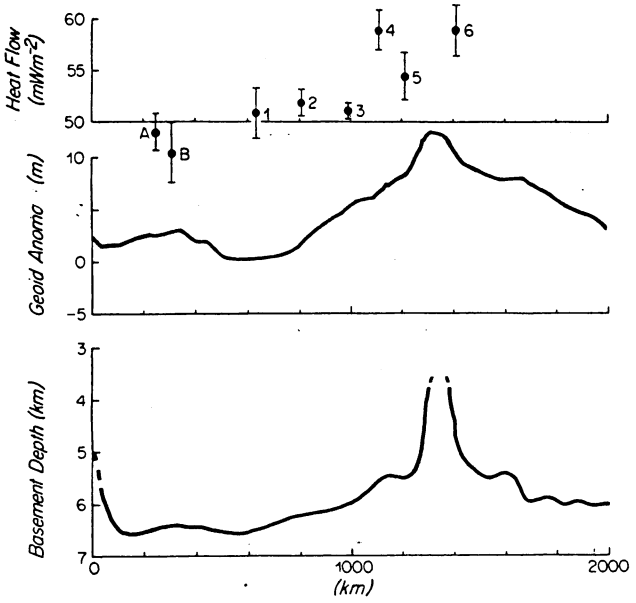

Fig. 11. Site mean heat flow values, geoid anomaly, and basement depth along the profile shown in Figure 3. Basement depths (uncorrected for sediment loading) from Tucholke et al. [1982].

ment depths off the Bermuda Rise; the off-swell sites still average 200-300 m shallower than predicted.

These observations cannot be explained by a simple adjustment of the parameters in the plate model such as equilibrium plate thickness, average mantle temperature, or thermal conductivity. For example, while a smaller equilibrium plate thickness would explain the anomalously shallow depths south and west of the Bermuda Rise, it would also predict a much earlier departure from the $t^{1/2}$ depth-age relation than that observed by Parsons and Sclater [1977] in the North Atlantic. In fact, no single set of plate or boundary layer model parameters can explain both the observed depth-age relation on the younger flanks of the Mid-Atlantic Ridge and the anomalously shallow depths of the old seafloor south and west of the Bermuda Rise. Purely conductive cooling, like that in the plate and boundary layer models, thus cannot completely explain the observed depths and heat flow in the western North Atlantic, even away from such clearly anomalous features as the Bermuda Rise.

The second important conclusion that we can draw from our results is that the heat flow on the Bermuda Rise is significantly higher than the surrounding seafloor and is well-correlated with the depth and geoid anomalies associated with this feature (Figure 11). The average heat flow at sites 4, 5, and 6 is 57.4 ± 2.6 mW m^{-2} compared to 49.5 ± 1.7 mW m^{-2} for the eight sites located off the swell. However, the strongest evidence in support of a heat flow anomaly on the Bermuda Rise is the low value observed at site D off the swell on crust with a similar age to sites 4, 5, and 6 on the swell. If we accept site D as providing a representative heat flow value for 120 Ma seafloor, then the amplitude of the heat flow anomaly associated with the Bermuda Rise is 8-10 mW m^{-2} or about 15-20% higher than the background heat flux.

It is interesting to note that both the observed heat flow on the Bermuda Rise (~57 mW m^{-2}) and the magnitude of the anomalous heat flow are comparable to that found along the older portion of the Hawaiian Swell near Midway [Detrick et al., 1981; Von Herzen et al., 1982].

The average heat flow measured on the Bermuda Rise is also in good agreement with the value of 57 mW m^{-2} measured by Hyndman et al. [1974] in a borehole on Bermuda (triangle in Figure 10). Hyndman et al. [1974] argued that higher radioactive heat production in the seamount could contribute as much as 4 mW m^{-2} to the excess heat flow. However, even if this estimate is correct (and it is based on an average radioactive heat production extrapolated from drilling only the upper 15% of the seamount), the residual heat flux (53 mW m^{-2}) is still significantly greater than the value of 47 mW m^{-2} measured at site D on similarly aged seafloor off the rise. Moreover, it is unlikely that higher crustal radioactive heat production is responsible for the higher heat flow observed on the surrounding swell since there is no evidence (e.g., substantial crustal thickening) to suggest that the whole Bermuda Rise was intruded by the lamprophyric sheets drilled on Bermuda.

Model Calculations

Although our immediate concern in this paper is to interpret the heat flow, depth, and geoid anomalies associated with the Bermuda Rise, our general goal is a better understanding of the origin of all midplate swells. An underlying assumption in the following calculations is that all midplate swells result from a single physical process with differences in the characteristics of individual swells arising from differences in the age and absolute velocity of the lithosphere on which they occur. In discussing the results of our calculations we treat the Bermuda Rise and Hawaiian Swell, which occur on plates of widely differing velocity, as representative of a range of possible behaviors.

The existence of higher heat flow on the Bermuda Rise and Hawaiian Swell suggests that mid-ocean swells have a thermal origin. The observed effective depths of compensation of the swells [Haxby and Turcotte, 1978; Crough, 1978] require that temperature-induced density changes occur in the lower part of the thermal plate. These results exclude models in which a swell is formed isostatically by a thickened crust or by flexural uplift caused by volcanic loading. Deeper support mechanisms such as underplating basalt [Burke and Whiteman, 1973] or peridotite [Jordan, 1979] to the base of the lithosphere, or altering the lithosphere's composition [Haxby and Turcotte, 1978], would be consistent with the heat flow observations only if they were associated with substantial temperature increases, in which case the swell would still fundamentally have a thermal origin.

The plates must be heated from below to change the temperatures in the lower part of the plate and to provide a localized source of melt for any volcanism. This can be accomplished by a localized, hot upwelling in the mantle as the overlying plate moves over it. A complete treatment of the interaction of a convective upwelling with a moving plate would require a

TABLE 2. Consraints on Models of Bermuda Rise

Parameter	Value
Present height of swell	800-1000 m
Wavelength of swell	~2000 m
Anomalous heat flow on swell	8-10 mW m^{-2}
Peak geoid anomaly on swell	~6-8 m
Compensation depth of the swell	40-70 km[a]
Age of crust at Bermuda	114-118 Ma
Initial uplift of the swell	middle Eocene (45-50 Ma)[b]
Age of volcanism	late middle Eocene to early Oligocene (33-43 Ma)[b,c]
Submergence of island	late Oligocene (25 Ma)[b]
Total subsidence of swell	<100-200 m since the late Oligocene[c]

[a] Haxby and Turcotte [1978], and Crough [1978]
[b] Tucholke and Mountain [1979]
[c] Reynolds and Aumento [1974]

full three-dimensional, variable viscosity, time-dependent convection calculation. At present, three-dimensional convection calculations are practical only in the simplest cases. We therefore consider two different and more restricted calculations. The first approach is to represent the heat source in an ad hoc manner in order to obtain a three-dimensional temperature structure [Von Herzen et al., 1982; Sandwell, 1982]. The primary goal in this case is to understand the temporal response of the lithosphere to a reheating event and the effect of plate velocity on the shape of the swell. In order to study the interaction of convection and the overlying lithosphere we also consider a two-dimensional calculation for convection beneath a rigid, stationary lid. The goal in this case is to determine whether the temperature changes associated with convective heating are sufficient to explain the magnitude of the heat flow, depth, and geoid anomalies over the Bermuda Rise.

The principal observational constraints on the Bermuda Rise which any successful model for its origin must explain are summarized in Table 2. These include the amplitude (800-1000 m) and wavelength (~2000 km) of the swell, the peak heat flow (8-10 mW m^{-2}) and geoid (6-8 m) anomalies, and an average compensation depth (40-70 km) within the thermally defined lithospheric plate. Other important constraints on the origin and geological history of the Bermuda Rise have been inferred from studies of sediments deposited on the surrounding sea floor [Tucholke and Mountain, 1979] and a drill hole on Bermuda [Reynolds and Aumento, 1974]. As described earlier, these results indicate that the Bermuda Rise has had a long history with the initial uplift beginning in the middle Eocene, some 45-50 m.y. ago, a relatively short period of active volcanism lasting from the late-middle Eocene (43 Ma) to the early Oligocene (33 Ma) followed by a long period of volcanic quiescence during which there has been little subsidence of Bermuda relative to sea level.

Lithospheric Reheating Models

Transient reheating, point source. Detrick and Crough [1978] and Crough [1978] proposed a simple transient reheating model to explain the uplift and subsidence of the Hawaiian Swell that involves the rapid motion of the Pacific plate across a fixed, steady state heat source in the sublithospheric mantle. In this model, the temperatures in the lower part of the thermal plate are instantaneously reset when the lithosphere passes over the hot spot by raising all temperatures beneath a given depth to the average mantle temperature. Detrick et al. [1981] and Von Herzen et al. [1982] showed that this model is consistent with the shape and amplitude of the heat flow anomaly associated with the Hawaiian Swell.

It is not immediately obvious that this model is applicable to Bermuda in light of its volcanic quiescence for the past 33 m.y. and the relatively slow motion of the North American plate in the hot spot reference frame [Morgan, 1983]. However, conceptually, this model is identical to that of a fixed plate subjected to a very short reheating event, i.e., a non-steady state heat source. The

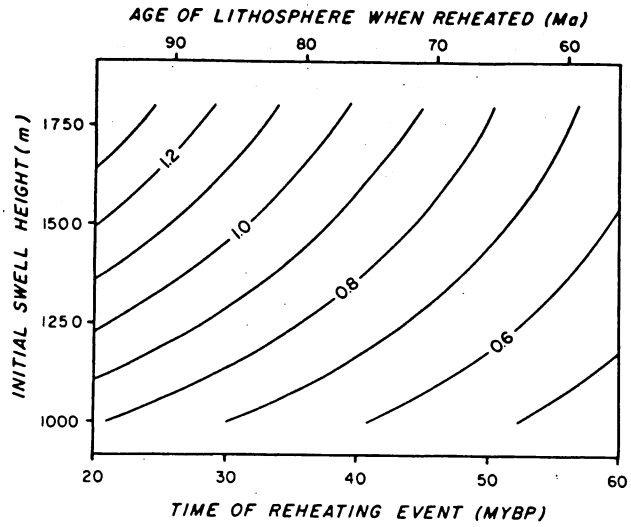

Fig. 12a. Contours (in kilometers) of present swell height as a function of initial swell height and time since reheating calculated using the analytical solution to the reheating problem described by Von Herzen et al. [1982]. If the reheating event is correlated with the volcanism on Bermuda at 33 Ma, then the present height of the Bermuda Rise (800-1000 m) requires an initial swell height of 1200-1550 m. The present age of the seafloor around Bermuda was assumed to be 116 Ma.

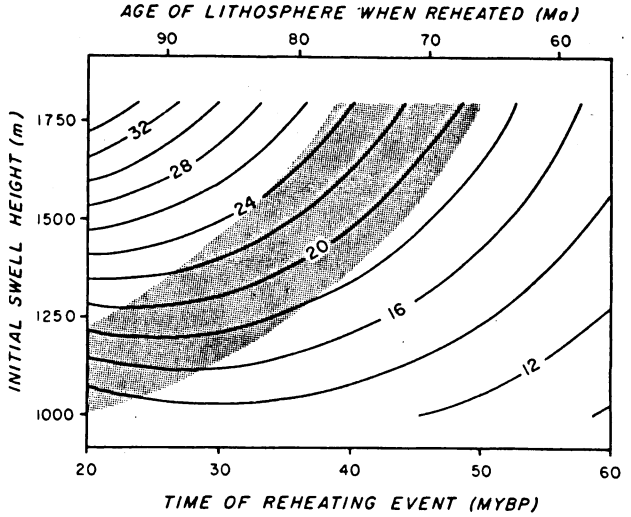

Fig. 12b. Same as Figure 12a except contours of present anomalous heat flow (in milliwatts per square meter) are shown. Shaded area indicates the predicted heat flow anomaly for initial swell heights that fit the present depths near the crest of the Bermuda Rise (Figure 12a). If the reheating event occurred at 33 Ma, the anomalous heat flow near the crest of the Bermuda Rise should be about 20 mW m^{-2}.

main difference in this case will be the absence of an elongate swell and island chain. Instead, the shape of the swell will reflect the cross-sectional area of the original heat source. In either case, Von Herzen et al. [1982] showed that the seafloor depth and heat flow at any time after the reheating event are completely determined by the geotherm (age) of the lithosphere when reheated and the initial swell height.

There are some difficulties in applying this model to Bermuda since neither the time of the reheating event or the initial height of the swell are well-known. For example, the reheating event could logically be placed anywhere between the middle Eocene (45-50 Ma) when the initial uplift of the Bermuda Rise began and 33 Ma, the date of the most recent volcanic activity on Bermuda. However, we can use the present height of the swell, the observed heat flow, and its subsidence history to constrain the range of acceptable solutions that are consistent with available geological evidence on the age of the Bermuda Rise.

In Figure 12a, for example, the predicted height of the rise is plotted as a function of the initial swell height and time since reheating. In calculating these curves we have assumed an age of 116 Ma for the crust around Bermuda and a plate model geotherm for the lithosphere prior to reheating. However, the use of a slightly different crustal age for the seafloor around Bermuda or a boundary layer geotherm would not significantly change the results. Similar plots are shown in Figures 12b and 12c for the anomalous heat flow on the swell and the expected swell subsidence. The latter has been calculated since the late Oligocene (25 Ma) when the Bermuda platform is believed to have sunk below sea level [Tucholke and Mountain, 1979].

The crest of the Bermuda Rise today stands 800-1000 m above the surrounding seafloor. If the reheating event is correlated with the last period of active volcanism on Bermuda at 33 Ma, then the initial swell height would have been 1200-1550 m to explain the present height of the rise. For

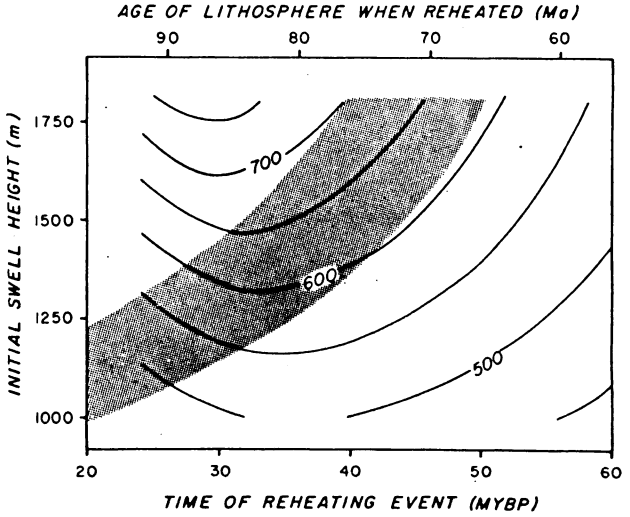

Fig. 12c. Same as Figure 12a except contours of total subsidence (in meters) since the late Oligocene (25 Ma) are shown. Shaded area indicates predicted subsidence for initial swell heights that fit the observed present height of the Bermuda Rise (Figure 12a). If the reheating event occurred at 33 Ma, the predicted subsidence at Bermuda is about 600-650 m.

these initial swell heights, the anomalous heat flow near the crest of the Bermuda Rise should be ~20 mW m^{-2} (Figure 12b), and the total subsidence of Bermuda since the late Oligocene should be 600-650 m (Figure 12c). If the reheating event occurred significantly earlier than 33 Ma, the initial swell height could be as great as 2000 m, and the present predicted heat flow and subsidence would be even larger.

It is difficult to reconcile these predictions with our observations on the Bermuda Rise and the characteristics of other known midplate swells. First, the initial swell height required to explain the present, relatively shallow depth of the Bermuda Rise is exceptionally large. The height of midplate swells varies according to the age of the seafloor on which they occur, with the higher ones formed on older lithosphere [Crough, 1978; Menard and McNutt, 1982]. However, compilations like that of Crough [1983b] indicate that even the largest swells usually rise no higher than about 1200-1300 m. Thus if this model is correct, it implies that the Bermuda Rise was once an unusually high swell, indicating an exceptionally large thermal anomaly. This inference is difficult to reconcile with the short eruptive history of Bermuda and its long period of volcanic inactivity. The predicted anomalous heat flow on the Bermuda Rise (~20 mW m^{-2}) is also substantially greater than what is observed (8-10 mW m^{-2}). To match the observed heat flow, the initial swell height would have to be less than 1000 m, which is inconsistent with the present height of the Bermuda Rise. However, the most difficult observation to reconcile with this model is the small amount of post-late Oligocene subsidence on Bermuda inferred from the minimal thickness of its coral reef cap [Reynolds and Aumento, 1974]. Given the long time which has elapsed since the reheating event which formed the Bermuda Rise (>30 Ma), a significant amount of subsidence (>500 m) is predicted regardless of the initial swell height (Figure 12c). While the magnitude and even the sign of eustatic sea level changes since the late Oligocene are controversial [M. Arthur, personal communication, 1985], we can probably rule out this amount of subsidence at Bermuda.

Transient reheating, distributed heat source. One major assumption in the previous analysis is that the lithosphere is thinned instantaneously over what is effectively a point heat source in the underlying mantle. Although swells, like that around Hawaii, appear to form quite rapidly (<10 Ma), the heat source must actually be distributed over a broad area nearly as wide as the swell itself, since lateral heat conduction will not be important over this very short period of time [Detrick and Crough, 1978]. Crough [1978] has shown that swells like Hawaii and Bermuda have a Gaussian-shaped bathymetric cross section with a half width of 400-600 km, and we may infer from the above argument that the underlying mantle heat source is probably of similar dimensions.

In the case of Hawaii, the distributed nature of the heat source might not be important since the Pacific plate is moving very rapidly (90 mm yr^{-1}) relative to the Hawaiian hotspot [Jarrard and Clague, 1977], and, at most, it will take only a few million years for the plate to pass over a heat source with a diameter as large as 600 km. However, this is not true of Bermuda. Most absolute plate motion solutions indicate that the North American plate is moving very slowly relative to hot spots, averaging about 15 mm yr^{-1} over the past 50 Ma (e.g., Morgan [1983]; see Figure 1). Thus it will take the North American plate at least 40 Ma to pass over a heat source 600 km across.

TABLE 3. Definitions and Values of Thermal Model

Parameters	Definitions	Values
α	thermal expansion coefficient	3.1×10^{-5} $^{o}C^{-1}$
D	flexural rigidity	7×10^{22} N m
C_p	heat capacity	1172 J kg^{-1} $^{o}C^{-1}$
K	thermal diffusivity	8×10^{-7} m^2 s^{-1}
ρ_m	mantle density	3330 kg m^{-3}
T_m	mantle temperature	1365°C

In order to assess quantitatively the importance of a distributed heat source on the predicted depth, heat flow, and geoid anomalies at Bermuda we have employed the Green's function technique developed by Sandwell [1982]. In this model, lithospheric reheating is simulated by increasing the temperature of the lower two thirds of the thermal plate (40-128 km depth) to a nearly constant value. The heat source q(x,y) varies as a Gaussian function in both horizontal directions:

$$q(x,y) = \left(\frac{\rho_m C_p V_x T_m f}{(2\pi)^{\frac{1}{2}}\sigma}\right)\exp\left(\frac{-(x^2+y^2)}{2\sigma^2}\right) \qquad (2)$$

where 2σ is the source half width, V_x is the plate velocity, and f is a number <1. The definitions and assigned values of the other model parameters are given in Table 3.

The amplitude of this source depends upon the thermal parameters ρ_m, C_p, and T_m and increases linearly with plate velocity V_x. The variation of source strength with plate velocity is an arbitrary assumption, but it is qualitatively consistent with geological evidence which suggests that the Bermuda hot spot has been much less active than the Hawaiian hot spot. Assuming that heat does not diffuse away from the source region, this amplitude factor ensures that the lower two thirds of the lithosphere will reach a temperature that is constant with depth ($fT_m\exp[y^2/2\sigma^2]$) after it passes over the source. Results were calculated for plate velocities of 90 mm yr^{-1} (Hawaii) and 15 mm yr^{-1} (Bermuda) assuming a source half width of 600 km. The value of f was chosen so as to produce a maximum initial swell height of 1400 m for the Hawaiian (90 mm yr^{-1}) model. The model parameters assumed were identical for both cases; the only difference was the absolute plate velocity relative to the heat source. In applying this model to Bermuda we have assumed that the heat source is steady state; however, the only real requirement is that the source strength

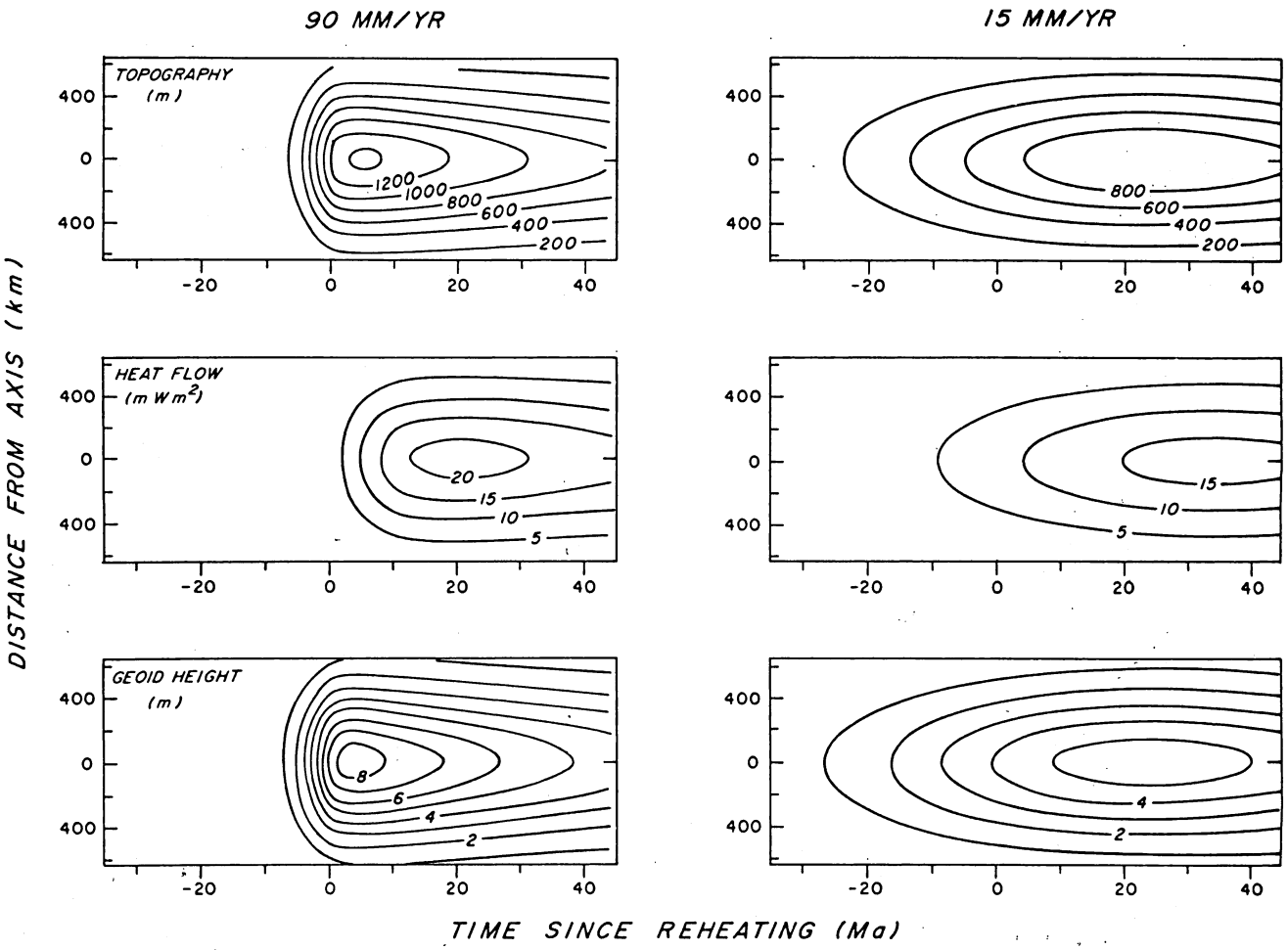

Fig. 13. Contours of anomalous depth, heat flow, and geoid height plotted against time since a moving plate passed over the center of a Gaussian-shaped heat source with 2σ = 600 km. Assumed plate velocities are 90 mm yr^{-1} (left) and 15 mm yr^{-1} (right). All other parameters were the same for both cases. Note the differences in swell shape, uplift, and subsidence depending on the velocity of the overriding plate. The results on the left would correspond to the Hawaiian Swell, those on the right to the Bermuda Rise.

remain the same during the time Bermuda passed over the hot spot. Even if the strength of the thermal anomaly has waned significantly since then (i.e., from 10 to 50 Ma) our predictions for Bermuda should still be valid.

The results are shown in Figure 13 in the form of contours of anomalous depth, heat flow, and geoid anomaly plotted against age. There are clearly major differences in the response of the lithosphere to a distributed heat source depending on the absolute velocity of the overriding plate. In each case the maximum depth, heat flow, and geoid anomalies are swept downstream by the moving lithosphere. However, for a slow moving plate the displacement in time between the source and the peak anomalies is significantly greater than for a fast moving plate, especially for the depth and geoid anomalies. The uplift and subsidence histories of the swell are also substantially different for these two cases. With a fast moving plate the swell is uplifted very rapidly: it remains shallow for a short period of time and then begins to subside. In contrast, swells formed on a slow moving plate are characterized by a long period of gradual uplift and an equally gradual subsidence. As a result, swells on these plates will remain shallow for tens of millions of years.

These differences are more clearly illustrated in Figure 14 where the peak depth and heat flow anomalies along the axis of the swell are plotted as a function of age (dotted curve, 15 mm yr^{-1}; dashed curve 90 mm yr^{-1}). For comparison, the predicted variation in these anomalies for the instantaneous reheating model discussed in the previous section are also shown (solid curve). As expected, the latter model provides a good approximation to the uplift and subsidence of swells formed on plates moving rapidly relative to hotspots. The main differences are that with a distributed heat source. the uplift begins 5-10 m.y. before the plate passes over the center of the heat source and the minimum swell depth is shifted slightly downstream of the center of the hot spot (Figure 14, top). These predictions are actually in good agreement with the observed variation in depth along the Hawaiian Swell [see Detrick et al., 1981, Figure 3]. Even for a fast moving plate, the predicted heat flow for a distributed heat source is substantially lower than for the point source model (Figure 14, bottom).

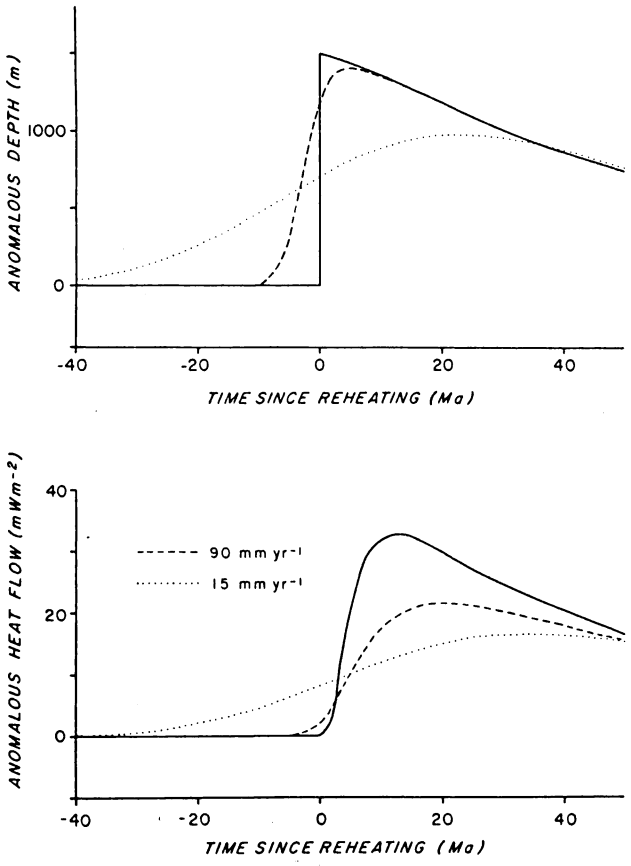

Fig. 14. Anomalous depth (top) and heat flow (bottom) as a function of time since reheating along the axis of the swells shown in Figure 13. The predictions are for a Gaussian-shaped heat source with 2σ = 600 km for a plate moving at both 90 mm yr^{-1} (dashed line) and 15 mm yr^{-1} (dotted line). For comparison, the anomalous depth and heat flow predicted by the instantaneous reheating model of Von Herzen et al. [1982] are also shown by the thick solid line.

This is because the extra heat is added to the lithosphere over several millions of years rather than all at once, allowing time for additional heat to diffuse out of the surface. For example, 10 m.y. downstream of the hot spot the predicted heat flow for the 90 mm yr^{-1} model is 17% less than calculated using the simple, instantaneous reheating model and at 20 m.y. the difference is still more than 10%. This may explain why the model curves published by Detrick et al. [1981] and Von Herzen et al. [1982] slightly overestimate the observed heat flow on the Hawaiian Swell.

For a plate that is moving slowly relative to hot spots, like the North American plate, the effect of the distributed nature of the heat source cannot be ignored. Not only are the magnitudes of the depth, heat flow, and geoid anomalies less, but also the entire uplift and subsidence history of the swell is completely different. For the cases illustrated in Figure 13, the peak depth and geoid anomalies are about one third less for the slow moving plate, while the peak heat flow anomaly is almost 25% smaller. The swell on the slow moving plate is uplifted gradually over 20 m.y. or more, and it remains shallow with very little subsidence for tens of millions of years (Figure 14, top). The shape of the swell will also be quite different. While swells on fast moving plates can extend for several thousand kilometers downstream of the hot spot, swells formed on plates with slow absolute motions will be much more circular in cross section, reflecting the dimensions of the underlying heat source (Figure 15).

If we correlate the volcanism on Bermuda at 33 Ma with the time Bermuda passed over the center of the heat source (0 m.y. in Figure 14) then this model predicts the initial uplift of the swell began 10 to 15 m.y. earlier, in the middle Eocene. This is in good agreement with the timing of the initial uplift of the Bermuda Rise inferred by Tucholke and Mountain [1979]. The distributed heat source model also predicts a present swell height of more than 900 m and a total subsidence of less than 100 m over the past 25 m.y., both of

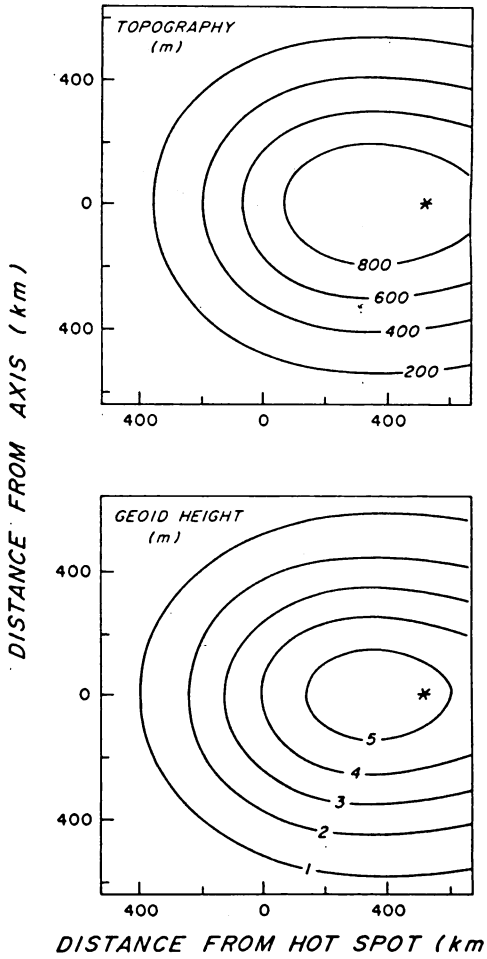

Fig. 15. Depth and geoid anomalies replotted from Figure 13 as a function of distance, instead of time, for an absolute plate velocity of 15 mm yr^{-1}. The star indicates the present position of Bermuda assuming it passed over the center of a steady state heat source at 33 Ma. Note the much more circular shape of the swell compared to Hawaii and the position of Bermuda close to the crest of the swell despite its relatively old age.

which agree with observations at Bermuda (Table 2). The magnitude of the predicted heat flow anomaly is comparable to, although somewhat larger than, that observed near Bermuda.

Convection Beneath a Conducting Lid

In the previous analysis we employed a relatively ad hoc heat source in order to determine the effect of absolute plate velocity on the depth, heat flow, and geoid anomalies associated with swells. In this section we investigate whether the temperature changes associated with convective heating are sufficient to explain the magnitude of these anomalies. A simple representation of the interaction of convective heating with a rigid plate is provided by convection in a layer of uniform viscosity beneath a conducting lid. The calculation is restricted to two dimensions. Since the Bermuda Rise is an approximately equidimensional feature, at least compared to the Hawaiian Swell, a two-dimensional calculation is probably appropriate. The governing equations were solved using standard finite difference methods [Richter, 1973]. Solutions of the equations of motion and continuity were obtained for the fluid layer with boundary conditions of zero normal velocity and zero shear stress on both top and bottom boundaries. A no-slip boundary condition might be considered more appropriate. However, as we discuss later, the existence of a low-viscosity zone beneath the lid is probably an important part of any general explanation of mid-ocean swells. For sufficiently low viscosities this will appear to the rest of the layer as an approximately stress-free boundary.

The heat transport equation was used to update simultaneously temperatures in both the convecting layer and conducting lid, velocities in the latter being taken to be zero. A constant heat flux was applied to the bottom boundary of the convecting layer and the top boundary of the conducting lid was fixed at a temperature equal to 0. The nature of the solutions is primarily governed by the Rayleigh number,

$$Ra = \frac{g \alpha F d^4}{k \kappa \gamma} \qquad (3)$$

where g is the gravitational acceleration, α the volume coefficient of thermal expansion, F the heat flux heating the layer from below, k the thermal conductivity, K the thermal diffusivity, and γ the kinematic viscosity of the fluid. In the example given, the values of the physical parameters used were $g = 10$ m s^{-2}, $\alpha = 2 \times 10^{-5}$ ^{o}K^{-1}, $k = 4.2$ W m^{-1} ^{o}K^{-1}, $K = 10^{-6}$ m^2 s^{-1}, $F = 42$ mW m^{-2} (1 HFU), and $d = 600$ km. The choice of the depth of the layer corresponds to upper mantle convection; its effect on the results of the calculation are discussed further below. Isotherms and streamlines for a steady state solution with $Ra = 4 \times 10^6$ and an aspect ratio of 1.5 are shown in Figure 16.

The surface heat flow can be calculated from the temperatures using a finite difference approximation to the temperature gradients in the conducting lid. The depth and geoid anomalies were calculated in a similar manner to that used for a constant viscosity layer [Parsons and Daly, 1983]. For a convecting system in which the equations of motion are linear, it can be shown

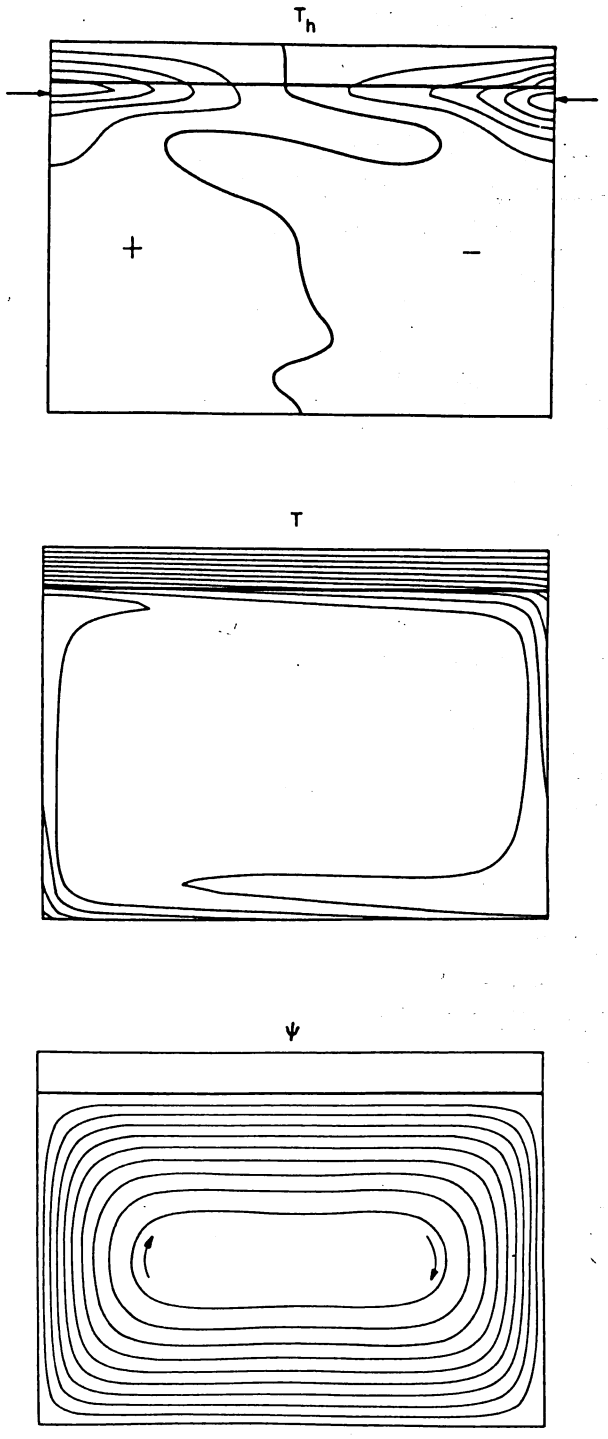

Fig. 16. Streamlines (ψ), temperature (T), and effective temperatures related to surface topography (T_h) for steady-state convection beneath a conducting lid driven by a constant heat flux or the bottom boundary of the layer with $Ra = 4 \times 10^6$. The solution was obtained on a uniform grid with 72 grid intervals in the horizontal, 48 grid intervals vertically across the convecting region, and 6 grid intervals across the lid. The contour values are ψ -133(14.8)0 in nondimensional units; T, 0(100)1300^{o}C; and T_h, -240(30)120. The first and last figures are the minimum and maximum contour values, with the value in parentheses the contour interval.

that a single wavelength component of surface topography, h(k), can be expressed as

$$h(k) = \frac{\rho_o \alpha}{(\rho_c - \rho_w)} \int_o^{d+\ell} H(k,z)T(k,z)dz \qquad (4)$$

where k is the wave number, ℓ the lid thickness, ρ_o the mantle density, and ρ_w the density of the seawater overlying the lid. T(k,z) is the variation with depth of the component of the temperature structure with the same horizontal wave number, k, as the topography. The kernel H in this integral relation can be derived from Green's function solutions of the equations of motion [Parsons and Daly, 1983]. The value of H varies from 1 at the upper boundary to 0 at the bottom boundary; the downweighting of temperature variations deeper in the layer represents the effect of shear stresses in balancing the buoyancy forces.

The geoid anomaly N(k) can be expressed in a similar fashion as

$$N(k) = \frac{2\pi G\rho_o \alpha}{\bar{g}k} \int_o^{d+\ell} G(k,z)T(k,z)dz \qquad (5)$$

where G is the gravitational constant and g is the mean value of gravity at the earth's surface. The gravity kernel G(k,z) includes the contributions to the gravity field from horizontal density variations and from topography on the top and bottom boundaries. Analytic expression for the kernels can be obtained for the case of a high-viscosity layer over a lower-viscosity layer (B. Parsons and S. Daly, manuscript in preparation, 1985). The geoid and depth anomalies associated with the temperature structure shown in Figure 16 were calculated using equations (4) and (5) with a thin lid approximation to the kernels. In this approximation the topography kernel H is equal to that for a constant viscosity layer with the appropriate boundary conditions everywhere beneath the lid and equal to 1 everywhere in the lid. This tends to overestimate somewhat the effects of shorter-wavelength temperature variations. The effects of the elastic properties of the lid were represented by including an additional factor

$$\phi(k) = [1+(k/\alpha)^4]^{-1} \qquad (6)$$

in the surface topography kernel where $\alpha^4 = [g(\rho_o-\rho_w)]/D$ and D is the flexural rigidity.

The heat flow, depth, and geoid anomalies produced by the convective temperature structure shown in Figure 16 are plotted in Figure 17. The magnitude of the calculated anomalies (heat flow ~ 15 mW m^{-2}, depth ~ 1.2 km, geoid ~ 10 m) are similar, though somewhat larger, than the observed anomalies over the Bermuda Rise.

The relationship between the calculated depth and geoid anomalies is consistent with apparent depths of compensation much shallower than the depth of the convecting layer and smaller than the thermal plate thickness. Consider variations in surface topography h with a wave number k that are compensated by an equal mass deficit concentrated at a single depth of compensation d_c. The resulting geoid anomaly N is the limit of long wavelengths for which $kd_c >> 1$ is

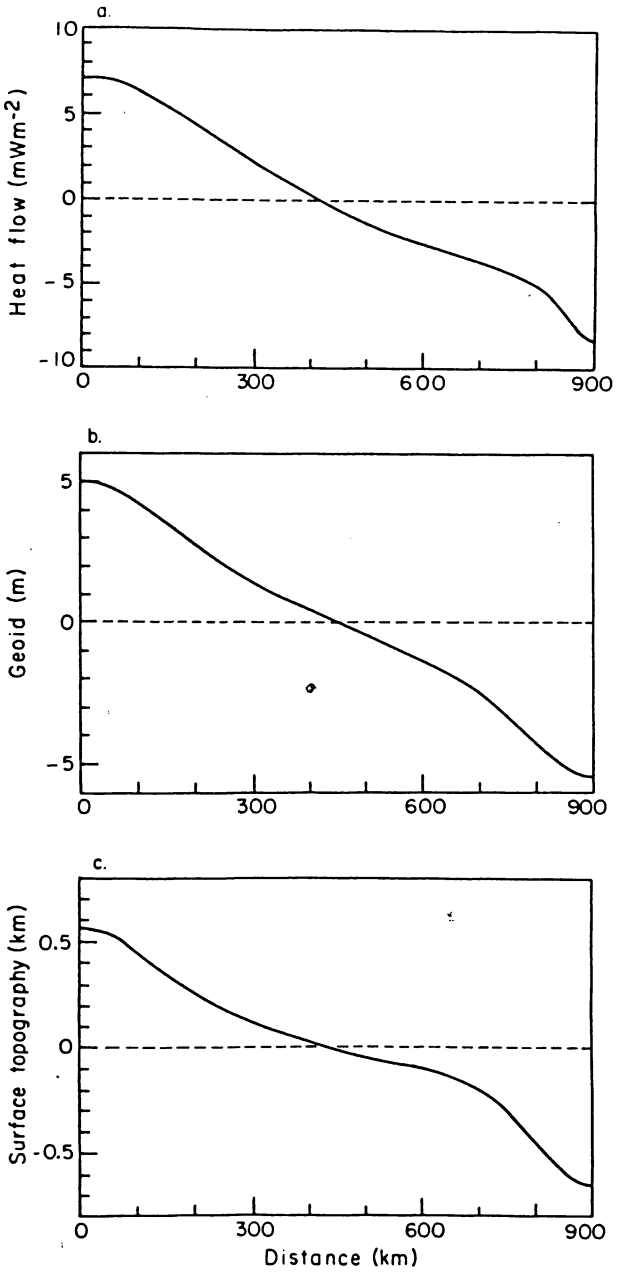

Fig. 17. (a) Heat flow, (b) geoid, and (c) topography calculated at the surface of the convecting region shown in Figure 16. The heat flow represents the variation about the mean value of 42 mW m^{-2} (1 HFU). The effects of an elastic plate with a flexural rigidity of 2 x 10^{23} N m, i.e., an elastic thickness of 30 km, were included in calculating the geoid and topography.

$$N = \left[\frac{2\pi G}{\bar{g}}(\rho_o-\rho_w)d_c\right]h \qquad (7)$$

This linear relation is independent of the wavelength, and its slope is proportional to the depth of compensation. In this way the approximately linear relationship between geoid and depth observed for profiles over the Bermuda Rise and Hawaiian Swell have been interpreted in terms of depths of compensation in the range 40-70 km

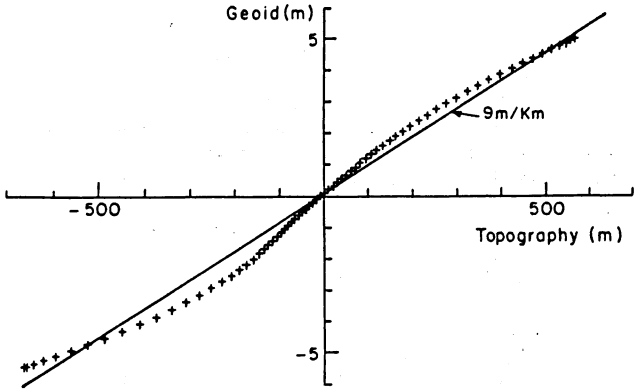

Fig. 18. Plot of geoid versus depth anomalies using the calculated observables from Figure 17. A straight line with a slope of 9 m km^{-1} is shown for reference.

[Haxby and Turcotte, 1978; Crough, 1978]. If the calculated geoid anomaly shown in Figure 17 is plotted versus the calculated surface topography, an approximately linear relation is also obtained (Figure 18). The apparent depth of compensation obtained from the slope of this relationship is indicated by the arrows in Figure 16.

The apparent depth of compensation is very shallow compared with the depth of the convecting layer, lying immediately beneath the base of the conducting lid. A simple explanation of this result can be given in terms of effective temperatures [Parsons and Daly, 1983]. The effective temperatures corresponding to the surface topography can be obtained by taking the inverse Fourier transform (F^{-1}) of equation (4):

$$(\rho_o-\rho_w)h(x) = \rho_o\alpha \int_o^{d+\ell} T_h(x,z)dz \qquad (8)$$

where the effective temperatures are given by

$$T_h(x,2) = F^{-1}\,[\,H(k,z)T(k,z)\,] \qquad (9)$$

Equation (8) has the form of a simple isostatic mass balance. The effective temperatures derived for the given examples using equation (9) are shown in Figure 16. The principal contributions to the depth and geoid anomalies come from regions where the effective temperature variations are concentrated, i.e., from the bottom of the conducting lid and in the thermal boundary layer beneath it. This point of view resolves the apparent conflict between models in which swells are explained in terms of a reheating of the lower part of the thermal plate [Detrick and Crough, 1978] and mantle convection models [McKenzie et al., 1980].

Because of the very simple nature of the model and the large number of parameters which affect the solution, we have not attempted to search for an exact match with the observed magnitudes of the heat flow, depth, and geoid anomalies over the Bermuda Rise. For instance, in the example given, the lid thickness is 75 km, forcing an apparent depth of compensation slightly greater than those observed. The choice of a thinner lid would correct this but would produce a larger heat flow anomaly and smaller depth and geoid anomalies. The heat flow anomaly can be reduced without changing the depth and geoid anomalies by reducing the thermal conductivity of the lid relative to that of the layer. In the calculation the physical parameters had the same value in both lid and layer. The magnitude of all three observables can be simultaneously reduced by decreasing the viscosity of the layer. Also the aspect ratio of the calculations affects the amplitude of the anomalies, larger aspect ratios tending to be associated with thicker boundary layers and larger temperature variations and hence larger amplitudes. A full exploration of the effect of the different parameters on the heat flow, depth, and geoid anomalies is described elsewhere (B. Parsons and S. Daly, manuscript in preparation, 1985).

The layer depth used corresponds to upper mantle convection. This choice is convenient in that it results in Rayleigh numbers for which solutions can be obtained without excessively large computations. If the depth were to be increased leaving other parameters unchanged the physical boundary layer thickness and temperature drop across it remain unchanged because of the way they scale with Rayleigh number. The contribution to the depth and geoid anomalies from the convecting region depends primarily on the upper boundary layer thickness and the temperature variations within it, as can be seen from the form of equations (4) and (5) and the effective temperature distributions derived using them. Consequently, the magnitude of the depth and geoid anomalies should not depend critically on the choice of layer depth. Finally, no special significance should be attached to the steady state nature of the solution given as an example here. The amplitudes of the anomalies shown are typical of solutions at this Rayleigh number. Thus we conclude that there is no difficulty in producing the observed magnitudes of heat flow, depth, and geoid anomalies over the Bermuda Rise with a convective heat source in the underlying mantle.

Summary

The predicted heat flow anomaly as a function of distance from Bermuda for both kinds of calculations described above are shown in Figure 19 where they are compared with the observed heat flow. The observed heat flow anomaly is largely confined to sites within about 300 km of Bermuda, although a small anomaly may exist up to 700 km from the island. Both the distributed heat source and convection calculations yield similar results. These models predict the general shape of the observed anomaly, although the heat flow near the crest of the swell is somewhat less than predicted. With the uncertainties in the various model parameters, this discrepancy may not be significant.

The two sets of calculations described above treat different aspects of the same problem and share certain basic assumptions. For example, in order to obtain agreement with the apparent depths of compensation derived from the observed geoid-depth relationships, it is necessary to identify the conducting lid in the two-dimensional convection calculations with the upper, rigid part of the thermal plate. In the lower part of the thermal plate, viscosities are assumed to be comparable to those in the underlying mantle, so that convection

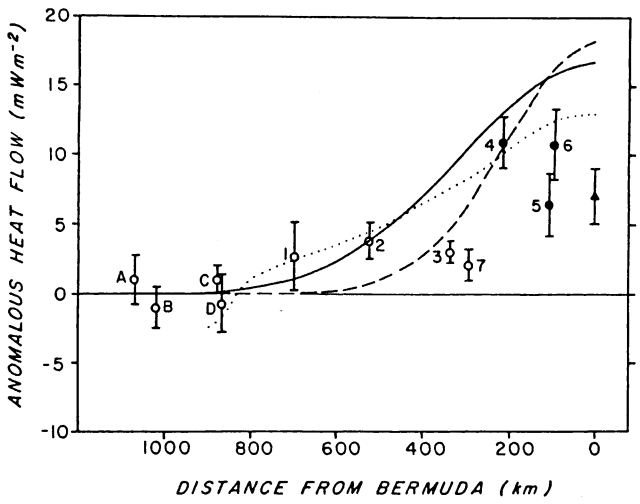

Fig. 19. Comparison of observed and predicted anomalous heat flux as a function of distance from Bermuda. Solid and dashed lines show the predicted heat flow for a slow (15 mm yr^{-1}) moving plate 35 m.y. after passing over a distributed heat source with 2σ = 600 km and 400 km, respectively. Dotted curve shows the predicted heat flow for the steady state convection model shown in Figure 18. Zero line has been arbitrarily set at 48 mW m^{-2}. Labeling of observed data as in Figure 10.

can transport hotter material into the lower part of the thermal plate, changing the temperatures there. The reheating model implicity makes the same assumption, distributing its heat source throughout the lower part of the thermal plate. This viscosity structure is the same as that used by Parsons and McKenzie [1978] in investigating possible convective instabilities arising from the cooling of the plates. Further studies of this phenomenon show that such a viscosity structure arises quite noticeably in materials with a temperature and pressure dependent viscosity [Yuen and Fleitout, 1987; Buck, 1985]. In fact, for reasonable values of the activation energy and volume that controls the temperature and pressure dependence, viscosities substantially lower than those beneath the plates are found at the base of the plate, forming a low-viscosity zone.

The existence of a low-viscosity zone at the base of the thermal plate would provide a means of merging the convection and reheating calculations, at least in principle. If the viscosity beneath the rigid lid was uniform everywhere, then motion of the lid with velocities comparable with that of the Pacific plate would result in convection beneath the lid being organized within reasonably short times into roll-like cells aligned with the direction of motion of the lid [Richter and Parsons, 1975]. However the history of the volcanism on the Hawaiian Swell seems to require a localized, approximately stationary source of melt. A low-viscosity zone would cause the horizontal velocities to vary most rapidly across it, leaving considerably reduced velocities in the mantle beneath it [Richter and McKenzie, 1978]. Roll-like convection could not then develop within a sufficiently short time, and localized, hot upwellings would occur at high Rayleigh numbers. When hot fluid nears the upper boundary, it will enter the low-viscosity zone, changing the temperatures in the lower part of the plate. Time-dependent calculations show that the amplitudes of the swell can be established over a short enough time if the viscosities are sufficiently low (B. Parsons and S. Daly, manuscript in preparation, 1985). At the same time, hot fluid would be swept downstream, and cooling by essentially vertical conduction then produces regular subsidence like that for the Hawaiian Swell [Detrick and Crough, 1978].

In reducing this general picture to the two simpler calculations, some conflicting assumptions have been made. In the reheating model, a heat source was introduced into the lower part of the thermal plate, temperatures changing in response to it. With a convective heat source, heating is provided by replacing material in the lower part of the plate with material that is already hotter. This difference can affect the early changes in geoid and depth anomalies. Also, in the reheating model the heat source was chosen such that temperatures are always less than the mean mantle temperature. With a convective heat source temperatures in the upwelling are in excess of the mean mantle temperature (Figure 16). With the larger temperatures at the base of the plate and a smoother distribution with depth than the reheating model, a convective source can produce a smaller heat flow anomaly associated with a given depth anomaly. Another difference is that with a convective heat source the temperature variations in the lower part of the plate will be associated with velocities away from the upwelling. For slow moving plates like the North American plate, these velocities will be comparable with that of the rigid plate. The reheating calculation assumes, however, that velocities in the lower part of the plate are equal everywhere to the surface velocity.

Despite the conflicting assumptions, two main conclusions can be drawn from these calculations. First, temperature changes produced by a convective upwelling are sufficient to explain the amplitudes of the heat flow, depth, and geoid anomalies over the Bermuda Rise. Second, differrences in the shape and subsidence history of swells like the Bermuda Rise and Hawaiian Swell can be explained by the interaction of the convective heat source with overlying plates of different absolute velocities. Two observations that remain difficult to explain are the lack of volcanism on or near Bermuda since 33 Ma and the orientation of the Bermuda Rise approximately orthogonal to Morgan's [1983] predicted hot spot track (see Figure 1). One possible explanation for both of these observations is that the Bermuda hot spot is a transient feature, sufficiently long-lived to explain the age and small amount of subsidence of the Bermuda Rise but without continuous upwelling from the mantle, producing a continuous supply of melt and a long hot spot track. With the slow absolute velocity of the North American plate in the fixed hot spot reference frame, the shape of the Rise thus may largely reflect the shape of the upwelling mantle material. Alternatively, the Bermuda hot spot may not be fixed as Morgan [1983] assumed, and the orientation of the Bermuda Rise may reflect the differential motion between it and the North American plate.

Conclusions

A field study of the geothermal flux on the Bermuda Rise and thermal and convection modeling of midplate swells lead to the following conclusions:

1. Purely conductive cooling, like that in the plate and boundary layer models, cannot completely explain the observed depths and heat flow in the western North Atlantic, even away from such clearly anomalous features as the Bermuda Rise. Unloaded basement depths for 150 Ma seafloor off the rise are 200-300 m shallower than predicted by either the plate or boundary layer model, and the heat flow appears to reach an equilibrium value of 48-50 mW m^{-2} by 120 Ma seafloor.

2. On the Bermuda Rise the heat flux is significantly higher (57.4 $\pm$ 2.6 mW m^{-2}) than off the swell (49.5 $\pm$ 1.7 mW m^{-2}). The magnitude of the anomalous heat flow (8-10 mW m^{-2}) associated with the Bermuda Rise is comparable to that previously found along the older portion of the Hawaiian Swell near Midway [Detrick et al., 1981; Von Herzen et al., 1982]. The existence of higher heat flow on both the Hawaiian Swell and Bermuda Rise indicates that these features have a thermal origin.

3. Thermal modeling of the bathymetry, heat flow, and subsidence history of the Bermuda Rise is consistent with the slow motion of the North American plate across a deep-seated, distributed heat source in the upper mantle. This model is consistent with the present relatively shallow depth of the Bermuda Rise, the amplitude of its associated heat flow and geoid anomalies and geological evidence for a long history of uplift and subsidence of the Bermuda Rise beginning in the middle Eocene, 45-50 Ma.

4. The major differences in the shape, uplift, and subsidence histories of the Hawaiian Swell and Bermuda Rise can be accounted for by the different absolute velocities of the Pacific and North American plates relative to hot spots. With a fast moving plate, swells are uplifted very rapidly, remain shallow for a short period of time, and then begin to subside. In contrast, swells formed on a slow moving plate are characterized by a long period of gradual uplift and equally gradual subsidence thus remaining shallow for tens of millions of years. While swells on fast moving plates will extend for several thousands of kilometers downstream of the hot spot, swells formed on plates with slow absolute motions will be much more circular in cross section, reflecting the dimensions of the underlying heat source.

5. Numerical studies of convection beneath a conducting lid show that the temperature variations associated with a convective upwelling can explain the magnitude of the depth, geoid, and heat flow anomalies over midplate swells. The observations are satisfied if the lower part of the thermally defined plate acts as the upper thermal boundary layer of the convection. These results suggest that convection is a likely mechanism for the lithospheric reheating associated with the formation of midplate swells.

Acknowledgments. We are indebted to the officers and crew of the R/V Knorr for their professional seamanship which made this experiment possible. G. Pelletier maintained and operated the heat flow instrumentation at sea, while P. Belknap and R. Handy were responsible for the seismic profiling system. N. Adams, C. Ebinger, J. Jemsek, N. Schulz, and M. Van Gool assisted with various stages of data reduction. The manuscript was skillfully typed by C. Sherman. This research was sponsored by National Science Foundation grant OCE20-17886 to the Woods Hole Oceanographic Institution with subcontracts to the Massachusetts Institute of Technology and the University of Rhode Island. Work on geoid and depth anomalies in the Atlantic Ocean at MIT has been supported by Office of Naval Research contract N00014-80-C-0273.

References

Anderson, R. N., D. McKenzie, and J. G. Sclater, Gravity, bathymetry, and convection in the earth, Earth Planet. Sci. Lett., 18, 391-407, 1973.

Anderson, R. N., M. G. Langseth, and J. G. Sclater, The mechanisms of heat transfer through the floor of the Indian Ocean, J. Geophys. Res., 82, 3391-3409, 1977.

Anderson, R. N., M. A. Hobart, and M.G. Langseth, Geothermal convection through oceanic crust and sediments in the Indian Ocean, Science, 204, 828-832, 1979.

Aumento, F., and J. M. Ade-Hall, Deep-Drill-1972: Petrology of the Bermuda drill core, Eos Trans. AGU, 54, 485, 1973.

Birch, F., R. F. Roy, and E. R. Dicker, Heat flow and thermal history in New England and New York, in Studies of Appalachian Geology: Northern and Maritime, edited by E. Zen, W. S. White, J. B. Haddley, and J. B. Thompson, Jr., pp. 437-451, Wiley Interscience, New York, 1968.

Buck, W. R., When does small-scale convection begin beneath ocenic lithosphere?, Nature, 313, 775-777, 1985.

Burke, K. C., and A. J. Whiteman, Uplift, rifting and the break-up of Africa, in Implications of Continental Drift to the Earth Sciences, edited by D. H. Tarling and S. K. Runcorn, pp. 735-755, Academic, Orlando, Fla., 1973.

Cochran, J. R., and M. Talwani, Gravity anomalies, regional elevation, and the deep structure of the North Atlantic, J. Geophys. Res., 83, 4907-4924, 1978.

Crough, S. T. Thermal origin of mid-plate hotspot swells, Geophys. J. R. Astron. Soc., 55, 451-469, 1978.

Crough, S. T., The correction for sediment loading on the seafloor, J. Geophys. Res., 88, 6649-6454, 1983a.

Crough, S. T., Hotspot swells, Annu. Rev. Earth Planet. Sci., 11, 165-193, 1983b.

Crough, S. T., and R. D. Jarrard, The Marqiesas-Line Swell, J. Geophys. Res. 86, 11763-11771, 1981.

Davis, E. E., and C. R. B. Lister, Heat flow measured over the Juan de Fuca ridge: Evidence for widespread hydrothermal circulation in a highly heat transportive crust, J. Geophys. Res., 82, 4845-4860, 1977.

Davis, E. E., C. R. B. Lister, and J. G. Sclater, Towards determining the thermal state of old ocean lithosphere: Heat flow measurements from the Blake-Bahama outer ridge, NW Atlantic,

Geophys. J. R. Astron. Soc., 78, 507-545, 1984.
Detrick, R. S., and S. T. Crough, Island subsidence, hot spots, and lithospheric thinning, J. Geophys. Res., 83, 1236-1244, 1978.
Detrick, R. S., R. P. Von Herzen, S. T. Crough, D. Epp, and U. Fehn, Heat flow on the Hawaiian swell and lithospheric reheating, Nature, 292, 142-143, 1981.
Embley, R. W., M. A. Hobart, R. N. Anderson, and D. Abbott, Anomalous heat flow in the northwest Atlantic: A case for continued hydrothermal circulation in 80 m.y. crust, J. Geophys. Res., 88, 1067-1074, 1983.
Galson, D. A., and R. P. Von Herzen, A heat flow survey on anomaly MO south of the Bermuda Rise, Earth Planet. Sci. Lett., 53, 296-306, 1981.
Gees, R. A., and F. Medioli, A continuous seismic survey of the Bermuda Platform, Marit. Sediments, 6, 21-25, 1970.
Haxby, W. F., and D. L. Turcotte, On isostatic geoid anomalies, J. Geophys. Res., 83, 5473-5478, 1978.
Hyndman, R. D., G. K. Myecke, and F. Aumento, Deep-Drill-1972, Heat flow and heat production in Bermuda, Can. J. Earth Sci., 11, 809-818, 1974.
Jarrard, R. D., and D. A. Claque, Implications of Pacific island and seamount ages for the origin of volcanic chains, Rev. Geophys 15, 57-76, 1977.
Johnson, G. L., and P. R. Vogt, Morphology of the Bermuda Rise, Deep Sea Res., 18, 605-617, 1971.
Jordan, T. H., Mineralogies, densities and seismic velocities of garnet lherzolites and their geophysical implications, in The Mantle Sample: Inclusions in Kimberlites and Other Volcanics, vol. 2, edited by F. R. Boyd and H. O. A. Meyer, pp. 1-14, AGU, Washington, D. C., 1979.
Kent, D. V., and F. M. Gradstein, A Jurassic to recent chronology, in The Geology of North America: The Western Atlantic Region, DNAG Series, edited by B. E. Tucholke and P. R. Vogt, Geological Society of America, Boulder, press, 1985.
Klitgord, K. D., and H. Schouten, Plate kinematics of the Central Atlantic, in The Geology of North America: The Western Atlantic Region, DNAG Series, edited by B. E. Tucholke and P. R. Vogt, Geological Society of America, Boulder, in press, 1985.
Larson, R. L., and T. W. C. Hilde, A revised time scale of magnetic reversals for the early Cretaceous and late Jurassic, J. Geophys. Res., 80, 2586-2594, 1975.
Lee, T. C. and T. L. Henyey, Heat-flow refraction across dissimilar media, Geophys. J. R. Astron. Soc., 39, 319-333, 1974.
LeDouaran, S., and B. Parsons, A note on the correction of ocean floor depths for sediment loading, J. Geophys. Res., 87, 4715-4722, 1982.
Lister, C. R. B., On the thermal balance of a mid-ocean ridge, Geophys. J. R. Astron. Soc., 34, 515-535, 1972.
Matthews, D. J., Tables of the velocity of sound in pure water and sea water, H. D. 282, 52 pp., Hydrogr. Dep., London, 1939.
McKenzie, D., The generation and compaction of partially molten rock, J. Petrol., 25, 713-765, 1984.
McKenzie, D., A. Watts, B. Parsons, and M. Roufosse, Planform of mantle convection beneath the Pacific Ocean, Nature, 288, 442-446, 1980.
Menard, H.W., Depth anomalies and the bobbing motion of drifting islands, J. Geophys. Res., 78, 5128-5137, 1973.
Menard, H. W., and M. K. McNutt, Evidence for and consequences of thermal rejuvenation, J. Geophys. Res., 87, 8570-8580, 1982.
Morgan, W. J., Plate motions and deep mantle convection, Mem. Geol. Soc. Am., 132, 7-22, 1972.
Morgan, W. J., Hotspot tracks and the early rifting of the Atlantic, Tectonophysics, 94, 123-139, 1983.
Parsons, B., and S. Daly, The relationship between surface topography, gravity anomalies and temperature structure of convection, J. Geophys. Res., 88, 1129-1144, 1983.
Parsons, B., and D. McKenzie, Mantle convection and the thermal structure of the plates, J. Geophys. Res., 83, 4485-4496, 1978.
Parsons, B., and J. C. Sclater, An analysis of the variation of ocean floor bathymetry and heat flow with age, J. Geophys. Res., 82, 803-827, 1977.
Ratcliffe, E. H., The thermal conductivities of ocean sediments, J. Geophys. Res., 65, 1535-1541, 1960.
Reynolds, P. H., and F. Aumento, Deep Drill 1972, Potassium-argon dating of the Bermuda drill core, Can. J. Earth Sci., 11, 1269-1273, 1974.
Richter, F. M., Dynamical models for sea floor spreading, Rev. Geophys., 11, 223-287, 1973.
Richter, F. M., and D. McKenzie, Simple plate models of mantle convection, J. Geophys. Res., 44, 441-471, 1978.
Richter, F. M., and B. Parsons, On the interaction of two scales of convection in the mantle, J. Geophys. Res., 80, 2529-2541, 1975.
Sandwell, D. T., Thermal isostasy: Response of a moving lithosphere to a distributed heat source, J. Geophys. Res., 87, 1001-1014, 1982.
Sclater, J. G., and L. Wixom, The relationship between depth and age and heat flow and age in the western North Atlantic, in The Geology of North America: The Western Atlantic Region, DNAG Series, edited by B. E. Tucholke and P. R. Vogt, Geological Society of America, Boulder, in press, 1985.
Spence, D. A., and D. L. Turcotte, Magma-drive propagation of cracks, J. Geophys. Res., 90, 575-580, 1985.
Tucholke, B. E., and G. S. Mountain, Seismic stratigraphy, lithostratigraphy and paleosedimentation patterns in the North American Basin, in Deep Drilling Results in the Atlantic Ocean: Continental Margins and Paleoenvironment, Maurice Ewing Series, vol. 3, edited by M. Talwani, W. Hay, and W. B. F. Ryan, pp. 58-86, AGU, Washington, D. C., 1979.
Von Herzen, R., and A. E. Maxwell, The measurement of thermal conductivity of deep-sea sediments by a needle-probe method, J. Geophys. Res., 64, 1557-1563, 1959.
Von Herzen, R. P., and S. Uyeda, Heat flow through the eastern Pacific Ocean floor, J. Geophys. Res., 68, 4219-4250, 1963.
Von Herzen, R. P., R. S. Detrick, S. T. Crough, D. Epp, and U. Fehn, Thermal origin of the Hawaiian swell: Heat flow evidence and thermal models, J. Geophys. Res., 87, 6711-6723, 1982.
Watts, A. B., Gravity and bathymetry in the cen-

tral Pacific Ocean, J. Geophys. Res., 81, 1533-1553, 1976.

Yuen, D. A., and L. Fleitout, Stability of oceanic lithosphere with variable viscosity: An initial-value approach, Phys. Earth Planet. Inter., 34, 173-185, 1984.

R. S. Detrick, Graduate School of Oceanography, Narragansett Bay Campus, University of Rhode Island, Kingston, RI 02881.

M. Dougherty, 122 Clark Building, WHOI, Woods Hole, MA 02543.

B. Parsons, Department of Earth, Planetary and Atmospheric Sciences, Massachusetts Institute of Technology, Cambridge, MA 02139.

D. Sandwell, Rockwall Rm. 426, National Geodetic Survey, National Ocean Service, NOAA, 6001 Executive Blvd., Rockville, MD 20852.

R. P. Von Herzen, Department of Geology and Geophysics, Woods Hole Oceanographic Institution, Woods Hole, MA 02543.

(Received May 20, 1985;
revised September 19, 1985:
accepted October 16, 1985.)